

SENSOR AND SIMULATION NOTES

Note 149

May 1972

NEAR FIELD OF SCATTERING BY A HOLLOW SEMI-INFINITE CYLINDER
AND ITS APPLICATION TO EMP STUDIES

by

CLEARED
FOR PUBLIC RELEASE
PL/PA 5/19/97

S. W. Lee, V. Jamnejad, and R. Mittra
Antenna Laboratory, University of Illinois
Urbana, Illinois 61801

ABSTRACT

Based on Wiener-Hopf techniques, the near field solution for scattering by a semi-infinite conducting tube due to a normally incident plane wave is obtained with extensive numerical results. Emphasis is given to the interpretation of the results in terms of the error in the measurement of the magnetic field due to the presence of the sensor boom. Guidelines for reducing such errors are suggested.

PL 96-1223

SENSOR AND SIMULATION NOTES

Note 149

May 1972

NEAR FIELD OF SCATTERING BY A HOLLOW SEMI-INFINITE CYLINDER
AND ITS APPLICATION TO EMP STUDIES

by

S. W. Lee, V. Jamnejad, and R. Mittra

Antenna Laboratory, University of Illinois

Urbana, Illinois 61801

ABSTRACT

Based on Wiener-Hopf techniques, the near field solution for scattering by a semi-infinite conducting tube due to a normally incident plane wave is obtained with extensive numerical results. Emphasis is given to the interpretation of the results in terms of the error in the measurement of the magnetic field due to the presence of the sensor boom. Guidelines for reducing such errors are suggested.

TABLE OF CONTENTS

Section	Page
1. INTRODUCTION.	1
2. FORMULATION OF THE PROBLEM.	3
3. SOLUTION OF WEINER-HOPF EQUATIONS	8
4. FACTORIZATION OF WIENER-HOPF KERNELS.	12
5. MAGNETIC FIELD AND DISTORTION PARAMETER	17
6. LOW-FREQUENCY APPROXIMATION	23
7. NUMERICAL RESULTS AND DISCUSSION.	26
8. CONCLUSION.	32
APPENDIX. DETAILS OF NUMERICAL COMPUTATIONS.	34
LIST OF REFERENCES.	57
FIGURES	59-75

1. INTRODUCTION

For measurements of the nuclear electromagnetic pulse (EMP) at high altitudes above the earth, the sensors often have to be mounted on a supporting boom that generally can be approximated by a conducting cylinder.^{1,2,3} Two important problems in this connection are the determination of the extent of field distortion due to the presence of the boom, and then the derivation of ways for minimizing this distortion. The present paper is a contribution to the first problem, namely, a study of the near field at the end of a semi-infinite conducting tube illuminated by a normally incident time-harmonic plane wave.

Using the Wiener-Hopf techniques, the semi-infinite tube problem has been investigated by a number of authors, namely Levin and Schwinger,⁴ Pearson,⁵ Vajnshtejn,⁶ Jones,⁷ Bowman,⁸ Einarsson et al.,⁹ and Kao.¹⁰ Some of these results are summarized in the books of Morse and Feshbach,¹¹ Noble,¹² Jones,¹³ and Mittra and Lee.¹⁴

The present paper makes two contributions to this problem. First, new formulas are derived for the factorization of the Wiener-Hopf kernels

$$L(\alpha) = \pi i J_1(\sqrt{k^2 - \alpha^2} a) H_1^{(1)}(\sqrt{k^2 - \alpha^2} a) \quad (1.1)$$

$$M(\alpha) = \pi i J_1'(\sqrt{k^2 - \alpha^2} a) H_1^{(1)'}(\sqrt{k^2 - \alpha^2} a). \quad (1.2)$$

It has long been recognized that the major difficulty in the semi-infinite tube problem lies in the numerical computations of the factorization of the kernels in Equation (1.1) and Equation (1.2). The conventional formula for factorization as used in references 3 through 12 leads to complicated

integrals and has hindered the generation of numerical data in the past. In the present work, the pole singularities of the Bessel functions and the branch singularities of the Hankel functions in Equation (1.1) and Equation (1.2) are treated separately; the factorization of the former yields an infinite product, while that of the latter leads to an infinite integral with a relatively simple integrand. Both the infinite product and the infinite integral converge fast enough to permit a convenient numerical evaluation by a computer. The second contribution of this paper is the study of the near field around the end of the semi-infinite tube, thus supplementing the works of other researchers who have considered the far field only.

The organization of the paper is as follows. In Section 2 the semi-infinite tube problem is formulated in a Wiener-Hopf equation and is subsequently solved in Section 3. The key step in the solution is the factorization of the two functions in Equation (1.1) and Equation (1.2), and that is accomplished in Section 4. In Section 5, the explicit expressions of the magnetic field and induced currents are given in the form of inverse Fourier integrals. At low frequency, however, the inverse Fourier integrals can be approximately evaluated and simple analytical formulas for the near field are derived in Section 6. For more general frequency range, we have to resort to numerical evaluation with the aid of a computer. Extensive results have been calculated and analyzed in Section 7; details of the numerical computations are given in the Appendix. Finally, a conclusion is given in Section 8.

2. FORMULATION OF THE PROBLEM

The geometry of a semi-infinitely long, conducting, hollow cylinder is shown in Figure 1. A plane wave is incident normally on the cylinder and is explicitly given by

$$H_x^{(i)} = e^{-ikz}, \quad E_y^{(i)} = \sqrt{\frac{\mu}{\epsilon}} H_x^{(i)} \quad (2.1)$$

where the time-factor $\exp(-i\omega t)$ has been dropped. The problem is to determine the scattered field defined by

$$\vec{H} = \vec{H}^{(t)} - \vec{H}^{(i)} \quad (2.2)$$

where $\vec{H}^{(t)}$ is the total field. First, we note that the incident tangential electric field can be written as

$$E_\phi^{(i)} = E_y^{(i)} \cos \phi = \sqrt{\frac{\mu}{\epsilon}} \frac{1}{2} (e^{i\phi} + e^{-i\phi}) e^{-ikz} \quad (2.3)$$

which is a superposition of two waves of the form

$$E_\phi^{(i)} = \sqrt{\frac{\mu}{\epsilon}} \frac{1}{2} e^{in\phi} e^{-ikz}, \quad n = \pm 1. \quad (2.4)$$

The circular symmetry of the cylinder preserves the ϕ -variation of the type $\exp(in\phi)$. Thus, in the following derivations, we will use Equation (2.4) instead of Equation (2.3) as the incident field, and only at the end (i.e., Section 5) will we combine the solutions with $n = \pm 1$ to obtain the desired results.

The scattered field will be decomposed into TE and TM waves with respect to z and is derivable from an electric potential $\psi^{(e)}$ and a magnetic potential $\psi^{(m)}$ through the following relations

$$\vec{E} = \frac{i}{\omega\epsilon} \nabla \times \nabla \times (\hat{z} \psi^{(e)}) - \nabla \times (\hat{z} \psi^{(m)}) \quad (2.5)$$

$$\vec{H} = \nabla \times (\hat{z} \psi^{(e)}) + \frac{i}{\omega\mu} \nabla \times \nabla \times (\hat{z} \psi^{(m)}) . \quad (2.6)$$

The potentials themselves satisfy the usual wave equation

$$\left[\frac{1}{\rho} \frac{\partial}{\partial \rho} \left(\rho \frac{\partial}{\partial \rho} \right) - n^2 + \frac{\partial^2}{\partial z^2} + k^2 \right] \psi(\rho, z) = 0 \quad (2.7)$$

where ψ stands for either $\psi^{(e)}$ or $\psi^{(m)}$, and is a function of ρ , ϕ , and z . However, since the ϕ -variation, namely $\exp(in\phi)$, is common to all field components, we have not explicitly indicated it in the argument of $\psi(\rho, z)$ in (2.7). Now, the problem is to solve Equation (2.7) subject to the following conditions:

$$(i) \quad (E_\phi, E_z) \text{ and } (H_\phi, H_z) \text{ are continuous across } \rho = a \text{ for } z > 0 \quad (2.8)$$

$$(ii) \quad (E_\phi^{(t)}, E_z^{(t)}) \text{ are identically zero at } \rho = a \text{ for } z < 0 \quad (2.9)$$

$$(iii) \quad E_z(\rho = a, z) \sim z^{-1/2}, \text{ as } z \rightarrow 0+ . \quad (2.10)$$

This can be accomplished by the Wiener-Hopf technique.

To this end, let us introduce the standard Fourier transform notations in the Wiener-Hopf technique:¹⁴

$$\Psi(\rho, \alpha) = \Psi_+(\rho, \alpha) + \Psi_-(\rho, \alpha) \quad (2.11)$$

$$\Psi_+(\rho, \alpha) = \int_0^\infty \psi(\rho, z) e^{i\alpha z} dz \quad (2.12)$$

$$\Psi_{-}(\rho, \alpha) = \int_{-\infty}^0 \psi(\rho, z) e^{i\alpha z} dz . \quad (2.13)$$

The Fourier transform of Equation (2.7) leads to

$$\left[\frac{1}{\rho} \frac{\partial}{\partial \rho} \left(\rho \frac{\partial}{\partial \rho} \right) - n^2 + \kappa^2 \right] \Psi(\rho, \alpha) = 0 \quad (2.14)$$

where $\kappa = \sqrt{k^2 - \alpha^2} = +i\sqrt{\alpha^2 - k^2}$ with its branch cuts shown in Figure 2.

In the region $\rho > a$, the solution of Equation (2.14) may be written in the form

$$\Psi^{(e)}(\rho, \alpha) = A(\alpha) H_n^{(1)}(\kappa\rho) \quad (2.15a)$$

for $\rho > a$

$$\Psi^{(m)}(\rho, \alpha) = \sqrt{\frac{\epsilon}{\mu}} B(\alpha) H_n^{(1)}(\kappa\rho) \quad (2.15b)$$

where $A(\alpha)$ and $B(\alpha)$ are unknowns to be found. Substituting Equation (2.15) into (2.5) and (2.6), we may obtain the expressions for the tangential components of the fields

$$E_{\phi}(\rho, \alpha) = \kappa A(\alpha) H_n^{(1)'}(\kappa\rho) + \frac{i n \alpha}{k \rho} B(\alpha) H_n^{(1)}(\kappa\rho) \quad (2.16)$$

$$E_z(\rho, \alpha) = \frac{i \kappa^2}{k} B(\alpha) H_n^{(1)}(\kappa\rho) \quad (2.17)$$

$$H_{\phi}(\rho, \alpha) = \sqrt{\frac{\epsilon}{\mu}} \left[-\kappa B(\alpha) H_n^{(1)'}(\kappa\rho) + \frac{i n \alpha}{k \rho} A(\alpha) H_n^{(1)}(\kappa\rho) \right] \quad (2.18)$$

$$H_z(\rho, \alpha) = \sqrt{\frac{\epsilon}{\mu}} \frac{i \kappa^2}{k} A(\alpha) H_n^{(1)}(\kappa\rho) . \quad (2.19)$$

Here $E_\phi(\rho, \alpha)$, for example, is the Fourier transform of $E_\phi(\rho, z)$. The prime on a Hankel function signifies the derivative with respect to its argument. From (2.16) through (2.19) we may derive two relations between the tangential electrical and magnetic fields at $\rho = a^+$, namely,

$$H_z(a^+, \alpha) = \frac{\sqrt{\frac{\epsilon}{\mu}} H_n^{(1)}(\kappa a)}{i\kappa k a H_n^{(1)\prime}(\kappa a)} \left[-\kappa^2 a E_\phi(a^+, \alpha) + n\alpha E_z(a^+, \alpha) \right] \quad (2.20)$$

$$H_\phi(a^+, \alpha) - \frac{n\alpha}{\kappa^2} H_z(a^+, \alpha) \equiv \sqrt{\frac{\epsilon}{\mu}} \frac{i\kappa}{\kappa} \frac{H_n^{(1)\prime}(\kappa a)}{H_n^{(1)}(\kappa a)} E_z(a^+, \alpha) . \quad (2.21)$$

These two relations will be used later in deriving the Wiener-Hopf equation.

Next consider the field in the region $\rho < a$. The solution of Equation (2.14) then takes the form

$$\Psi^{(e)}(\rho, \alpha) = C(\alpha) J_n(\kappa\rho) \quad (2.22a)$$

$$\rho < a .$$

$$\Psi^{(m)}(\rho, \alpha) \equiv \sqrt{\frac{\epsilon}{\mu}} D(\alpha) J_n(\kappa\rho) \quad (2.22b)$$

In a similar manner, we may derive

$$H_z(a^-, \alpha) = \frac{\sqrt{\frac{\epsilon}{\mu}} J_n(\kappa a)}{i\kappa k a J_n'(\kappa a)} \left[-\kappa^2 a E_\phi(a^-, \alpha) + n\alpha E_z(a^-, \alpha) \right] \quad (2.23)$$

$$H_\phi(a^-, \alpha) - \frac{n\alpha}{\kappa^2} H_z(a^-, \alpha) \equiv \sqrt{\frac{\epsilon}{\mu}} \frac{i\kappa}{\kappa} \frac{J_n'(\kappa a)}{J_n(\kappa a)} E_z(a^-, \alpha) \quad (2.24)$$

which are identical to (2.20) and (2.21) except that the Bessel functions instead of Hankel functions are used.

Now we will apply the boundary conditions in Equations (2.8) and (2.9) to the four Equations (2.20), (2.21), (2.23), and (2.24). The subtraction of Equation (2.23) from Equation (2.20) gives

$$V_-(\alpha) = \frac{-2i}{k(\kappa a)^2 M(\alpha)} [U_+(\alpha) + \kappa^2 a E_{\phi^-}^{(i)}(a, \alpha)] \quad (2.25)$$

with the notations defined as

$$M(\alpha) = \pi i J_n'(\kappa a) H_n'(\kappa a) \quad (2.26)$$

$$V_-(\alpha) \equiv \sqrt{\frac{\mu}{\epsilon}} [H_{z^-}(a^+, \alpha) - H_{z^-}(a^-, \alpha)] \quad (2.27)$$

$$U_+(\alpha) = -\kappa^2 a E_{\phi^+}(a, \alpha) + n\alpha E_{z^+}(a, \alpha) \quad (2.28)$$

$$E_{\phi^-}^{(i)}(a, \alpha) \equiv \sqrt{\frac{\mu}{\epsilon}} \frac{1}{2i(\alpha - k)} \quad (2.29)$$

Similarly the subtraction of Equation (2.24) from Equation (2.21) yields

$$U_-(\alpha) = \frac{2ik}{L(\alpha)} V_+(\alpha) \quad (2.30)$$

where

$$L(\alpha) = \pi i J_n(\kappa a) H_n^{(1)}(\kappa a) \quad (2.31)$$

$$U_-(\alpha) \equiv \sqrt{\frac{\epsilon}{\mu}} \left\{ n\alpha [H_{z^-}(a^+, \alpha) - H_{z^-}(a^-, \alpha)] - \kappa^2 a [H_{\phi^-}(a^+, \alpha) - H_{\phi^-}(a^-, \alpha)] \right\} \quad (2.32)$$

$$V_+(\alpha) = E_{z^+}(a, \alpha) . \quad (2.33)$$

We will attack the two Wiener-Hopf Equations in (2.25) and (2.30) in Section 3. Once that is accomplished, the complete field solution may be determined from the following relations:

$$A(\alpha) = \frac{-1}{\kappa^3 a H_n^{(1)}(\kappa a)} \left\{ U_+(\alpha) + \kappa^2 a E_{\phi^-}^{(i)}(a, \alpha) \right\} \quad (2.34)$$

$$B(\alpha) = \frac{k}{i\kappa^2 H_n^{(1)}(\kappa a)} V_+(\alpha) \quad (2.35)$$

$$C(\alpha) = \frac{-1}{\kappa^3 a J_n'(\kappa a)} \left\{ U_+(\alpha) + \kappa^2 a E_{\phi^-}^{(i)}(a, \alpha) \right\} \quad (2.36)$$

$$D(\alpha) = \frac{k}{i\kappa^2 J_n(\kappa a)} V_+(\alpha) \quad (2.37)$$

in which A, B, C, and D are the coefficients of the potentials defined in Equations (2.15) and (2.22).

3. SOLUTION OF WIENER-HOPF EQUATIONS

Let us first consider Equation (2.25) and seek the solution of $U_+(\alpha)$. One of the key steps is the factorization of $M(\alpha)$ such that

$$M(\alpha) = M_+(\alpha) M_+(-\alpha) \quad (3.1)$$

where $M_+(\alpha)$ is regular and free from zeros in the upper-half α -plane defined by $\text{Im } \alpha > (-\text{Im } k)$. This procedure will be discussed in detail in Section 4. Substituting Equation (3.1) in Equation (2.25), we have

$$(k - \alpha)k M_+(-\alpha) V_-(\alpha) = \frac{-2i}{(k + \alpha)a^2 M_+(\alpha)} U_+(\alpha) + \frac{\sqrt{\mu/\epsilon}}{a M_+(\alpha)}. \quad (3.2)$$

Note that the left-hand side of Equation (3.2) contains functions regular in the lower-half α -plane, defined by $\text{Im } \alpha < \text{Im } k$, while the right-hand side contains functions regular in the upper-half α -plane, defined by $\text{Im } \alpha > (-\text{Im } k)$. By analytic continuation, both sides must be equal to a polynomial, say, $P(\alpha)$:

$$\frac{-2i}{(k + \alpha)a^2 M_+(\alpha)} U_+(\alpha) + \frac{\sqrt{\mu/\epsilon}}{a M_+(\alpha)} = P(\alpha). \quad (3.3)$$

To determine $P(\alpha)$ we have to study the asymptotic behavior of Equation (3.3) as $|\alpha| \rightarrow \infty$ in the upper-half plane. From the edge condition in Equation (2.10), one may show that

$$E_{z+}(a, \alpha) \sim \alpha^{-1/2}, \quad E_{\phi+}(a, \alpha) \sim \alpha^{-3/2} \quad (3.4)$$

as $|\alpha| \rightarrow \infty$ with $\text{Im } \alpha > 0$.

Recalling the definition of $U_+(\alpha)$ in Equation (2.28), it follows that

$$U_+(\alpha) \sim \alpha^{1/2}, \quad |\alpha| \rightarrow \infty \text{ with } \text{Im } \alpha > 0. \quad (3.5)$$

As will be shown in Section 4, the asymptotic behavior of $M_+(\alpha)$ is of the form

$$M_+(\alpha) \sim \alpha^{-1/2}, \quad |\alpha| \rightarrow \infty \text{ with } \text{Im } \alpha > 0. \quad (3.6)$$

Making use of Equations (3.5) and (3.6) in Equation (3.3) leads to the conclusion that $P(\alpha)$ is a constant, say P_0 . Then Equation (3.3) becomes

$$U_+(\alpha) = \frac{a^2(k + \alpha) M_+(\alpha)}{-2i} \left[P_0 - \frac{\sqrt{\mu/\epsilon}}{a M_+(\alpha)} \right]. \quad (3.7)$$

For convenience of later manipulations, we will now express P_0 in terms of a particular value of $U_+(\alpha)$. Setting $\alpha = k$ in Equation (3.3) and solving for P_0 , we obtain the following result,

$$P_0 = \frac{\sqrt{\mu/\epsilon}}{a M_+(k)} - i \frac{U_+(k)}{a^2 k M_+(k)}. \quad (3.8)$$

Substitution of (3.8) into (3.7) leads to

$$U_+(\alpha) = (k + \alpha) M_+(\alpha) \left\{ \frac{U_+(k)}{2k M_+(k)} \mp \sqrt{\frac{\mu}{\epsilon}} \frac{a}{2i} \left[\frac{1}{M_+(\alpha)} - \frac{1}{M_+(k)} \right] \right\}. \quad (3.9)$$

The constant $U_+(k)$ will be determined later.

Next consider the solution of Equation (2.30). Again the key step is the factorization of $L(\alpha)$ such that

$$L(\alpha) = L_+(\alpha) L_+(-\alpha), \quad (3.10)$$

which will be detailed in Section 4. Similarly we may show that

$$U_-(\alpha) L_+(-\alpha) = \frac{2ik}{L_+(\alpha)} V_+(\alpha) = Q(\alpha) \quad (3.11)$$

in which $Q(\alpha)$ is a polynomial. Since

$$L_+(\alpha), V_+(\alpha) \sim \alpha^{-1/2}, \text{ and } U_-(\alpha) \sim \alpha^{1/2} \quad (3.12)$$

as $|\alpha| \rightarrow \infty$ in their respective half plane, it follows that $Q(\alpha)$ is also a constant. Then the solution of Equation (3.11) may be written as

$$V_+(\alpha) = \frac{L_+(k) U_-(-k)}{2ik} L_+(\alpha) . \quad (3.13)$$

Now we will determine the two constants $U_+(k)$ and $U_-(-k)$ in Equations (3.9) and (3.13).

From the definitions in Equations (2.27), (2.28), (2.32), and (2.33) we derive the relations

$$U_+(k) = nk E_{z+}(a, k) = nk V_+(k) , \quad (3.14)$$

$$U_-(-k) \equiv \sqrt{\frac{\epsilon}{\mu}} (-nk) [H_{z-}(a+, -k) - H_{z-}(a-, -k)] \quad (3.15)$$

$$= -nk V_-(-k).$$

$$= -\frac{n}{2ka} \frac{1}{M_+^2(k)} \left[1 - \frac{i}{ka} U_+(k) \right] .$$

In the last step in Equation (3.15) we have used Equations (3.2), (3.3), and (3.4). Setting $\alpha = k$ in Equation (3.13), and using Equations (3.14) and (3.15), we may obtain the following solution for the constant $U_+(k)$:

$$U_+(k) \equiv \sqrt{\frac{\mu}{\epsilon}} \frac{ika n^2 L_+^2(k)}{4(ka)^2 M_+^2(k) - n^2 L_+^2(k)} . \quad (3.16)$$

Then it follows from Equations (3.15) and (3.16) that

$$U_{-}(-k) \equiv \sqrt{\frac{\mu}{\varepsilon}} \frac{-2nka}{4(ka)^2 M_{+}^2(k) - n^2 L_{+}^2(k)} . \quad (3.17)$$

Substitution of Equations (3.16) and (3.17) into Equations (3.9) and (3.13) completely determines the solutions for $U_{+}(\alpha)$ and $V_{+}(\alpha)$. When these results are used in Equations (2.34) through (2.37), the desired solutions are obtained and are given below:

$$\begin{aligned} H_n^{(1)'}(\kappa a) A(\alpha) &= J_n'(\kappa a) C(\alpha) \\ &\equiv \sqrt{\frac{\mu}{\varepsilon}} \frac{2(ka)^2 M_{+}(k)}{N_{+}(k)} \frac{(k + \alpha)}{i(k^2 - \alpha^2)^{3/2}} M_{+}(\alpha) \end{aligned} \quad (3.18)$$

$$\begin{aligned} H_n^{(1)}(\kappa a) B(\alpha) &= J_n(\kappa a) D(\alpha) \\ &\equiv \sqrt{\frac{\mu}{\varepsilon}} \frac{nka L_{+}(k)}{N_{+}(k)} \frac{L_{+}(\alpha)}{(k^2 - \alpha^2)} \end{aligned} \quad (3.19)$$

in which

$$N_{+}(k) = 4(ka)^2 M_{+}^2(k) - n^2 L_{+}^2(k) .$$

The field solution computed from Equations (3.18) and (3.19) will be discussed in Section 5.

4. FACTORIZATION OF WIENER-HOPF KERNELS

A key step in solving the present problem by the Wiener-Hopf technique lies in the factorization of the following two functions

$$L(\alpha) = \pi i J_1(\sqrt{k^2 - \alpha^2} a) H_1^{(1)}(\sqrt{k^2 - \alpha^2} a) \quad (4.1)$$

$$M(\alpha) = \pi i J_1'(\sqrt{k^2 - \alpha^2} a) H_1^{(1)'}(\sqrt{k^2 - \alpha^2} a) \quad (4.2)$$

in a manner such that

$$L(\alpha) = L_+(\alpha) L_-(\alpha) = L_+(\alpha) L_+(-\alpha) \quad (4.3)$$

$$M(\alpha) = M_+(\alpha) M_-(\alpha) = M_+(\alpha) M_+(-\alpha) \quad (4.4)$$

where $L_+(\alpha)$ and $M_+(\alpha)$ are regular and free from zeros in the upper-half complex α -plane defined by $\text{Im } \alpha > (-\text{Im } k)$, and behave algebraically as $|\alpha| \rightarrow \infty$.

Let us first concentrate on the factorization of $L(\alpha)$. A standard formula for $L_+(\alpha)$ is expressed in terms of a Cauchy integral:

$$L_+(\alpha) = \exp \frac{1}{2\pi i} \int_{-\infty+ic}^{\infty+ic} \frac{\ln[\pi i J_1(\sqrt{k^2 - \beta^2} a) H_1^{(1)}(\sqrt{k^2 - \beta^2} a)]}{\beta - \alpha} d\beta \quad (4.5)$$

$$- \text{Im } k < c < \text{Im } \alpha < \text{Im } k .$$

A number of authors including Levine and Schwinger,⁴ Vajnshtejn,⁶ Jones,⁷ and Bowman⁸ have presented a variety of different formulas for $L_+(\alpha)$, all based on (4.5). In the present work, we will derive an alternative expression using a newly developed factorization formula; the result obtained is believed to be simpler and more suitable for numerical calculations.

First of all, we recognize that $L(\alpha)$ is a product of the following two functions

$$L^{(1)}(\alpha) = \pi i J_1(\sqrt{k^2 - \alpha^2} a) \quad (4.6)$$

$$L^{(2)}(\alpha) = H_1^{(1)}(\sqrt{k^2 - \alpha^2} a) . \quad (4.7)$$

Note that $L^{(1)}(\alpha)$ is a meromorphic function, its factorization can be achieved by expressing it in an infinite product form:

$$L^{(1)}(\alpha) = \pi i J_1(ka) \cdot \left(1 - \frac{\alpha^2}{k^2}\right)^{1/2} \cdot \prod_{m=1}^{\infty} \left(1 + \frac{\alpha^2}{\gamma_m^2}\right) \quad (4.8)$$

where

$$\gamma_m = \sqrt{(j_m/a)^2 - k^2} = -i \sqrt{k^2 - (j_m/a)^2}$$

$j_m =$ ordered zeros of $J_1(x)$.

Separating the zeros of $L^{(1)}(\alpha)$ in the upper and lower-half α -planes, we obtain immediately

$$L_+^{(1)}(\alpha) = \sqrt{\pi i} J_1(ka) \left(1 + \frac{\alpha}{k}\right)^{1/2} \prod_{m=1}^{\infty} \left(1 + \frac{\alpha}{i\gamma_m}\right) e^{i\alpha a/m\pi} \quad (4.9)$$

in which the exponential factor has been added to ensure the uniform convergence of the infinite product.

The function $L^{(2)}(\alpha)$ in Equation (4.7) has no zeros* and has only a pair of branch singularities in $\sqrt{\alpha^2 - k^2}$ with its branch cuts shown in

*The Hankel function $H_1^{(1)}(z)$ has zeros with negative imaginary parts, but $\sqrt{k^2 - \alpha^2}$ assumes only either positive real or positive imaginary values.

Figure 2. To factorize this function, we will use a new formula.¹⁴ Omitting the details of the application of this formula, the final result is

$$L_+^{(2)}(\alpha) = \sqrt{H_1^{(1)}(ka)} \left(1 + \frac{\alpha}{k}\right)^{-1/2} \exp \left[-\frac{ika}{2} + \frac{\sqrt{k^2 - \alpha^2}}{2} a \ln \alpha + \frac{i\sqrt{k^2 - \alpha^2}}{k} + q(\alpha) \right] \quad (4.10a)$$

where $q(\alpha)$ is in the form of an infinite integral

$$q(\alpha) = \frac{1}{\pi} \int_0^\infty \left[1 - \frac{2}{\pi x} \frac{1}{J_1^2(x) + Y_1^2(x)} \right] \ln \left(1 + \frac{\alpha a}{\sqrt{(ka)^2 - x^2}} dx \right). \quad (4.10b)$$

The bar on the integral signifies the principal value integral at the singularity $x = ka$. As will be discussed in the Appendix, this logarithmic singularity is such that Equation (4.10b) can be easily evaluated numerically.

The product of $L_+^{(1)}(\alpha)$ and $L_+^{(2)}(\alpha)$ gives

$$L_+(\alpha) = e^{\chi(\alpha)} L_+^{(1)}(\alpha) L_+^{(2)}(\alpha) \quad (4.11)$$

in which the exponential factor is added to ensure the algebraic behavior of $L_+(\alpha)$ as $|\alpha| \rightarrow \infty$, in the upper-half α -plane. To determine $\chi(\alpha)$, it is necessary to know the asymptotic behavior of $L_+^{(1)}(\alpha)$ and $L_+^{(2)}(\alpha)$. Omitting the details, the final results are, as $|\alpha| \rightarrow \infty$ with $\text{Im } \alpha > 0$:

$$L_+^{(1)}(\alpha) \sim \alpha^{-1/4} \exp \left\{ \frac{\alpha a}{\pi i} \left[1 - C - \ln \left(\frac{\alpha a}{\pi i} \right) \right] \right\} \quad (4.12)$$

$$L_+^{(2)}(\alpha) \sim \alpha^{-1/4} \exp \left(\frac{\alpha a}{\pi i} \ln \frac{2\alpha}{k} \right) \quad (4.13)$$

where $C = \text{Euler's constant} = 0.57721\dots$. It follows immediately that

$$\chi(\alpha) = \frac{i\alpha a}{\pi} \left[1 - C + \ln\left(\frac{2\pi}{ka}\right) + i\frac{\pi}{2} \right] \quad (4.14)$$

and

$$L_+(\alpha) \sim \alpha^{-1/2}, \quad |\alpha| \rightarrow \infty \text{ with } \text{Im } \alpha > 0. \quad (4.15)$$

The final result of the factorization of $L(\alpha)$ is given by

$$L_+(\alpha) = L_-(-\alpha) \quad (4.16)$$

$$= \sqrt{\pi i J_1(ka) H_1^{(1)}(ka)} \exp \left\{ \frac{i\alpha a}{\pi} \left[1 - 0.57721 + \ln\left(\frac{2\pi}{ka}\right) + i\frac{\pi}{2} \right] - i\frac{ka}{2} \right\} \\ \cdot \exp \left\{ \frac{i\alpha \gamma}{\pi} \ln\left(\frac{\alpha - \gamma}{k}\right) + q(\alpha) \right\} \prod_{m=1}^{\infty} \left(1 + \frac{\alpha}{i\gamma_m} \right) e^{i\alpha a/m\pi}$$

where $\gamma = \sqrt{\alpha^2 - k^2} = -i\sqrt{k^2 - \alpha^2}$; γ_m is defined in Equation (4.8) and $q(\alpha)$ in Equation (4.10b). The expression in Equation (4.16) seems to be simpler than those derived in all the previous references,³⁻¹² and can be readily evaluated numerically (cf., Appendix).

The factorization of $M(\alpha)$ in Equation (4.2) can be achieved in a similar fashion. Its final result is given below:

$$M_+(\alpha) = M_-(-\alpha) \quad (4.17a)$$

$$= \sqrt{\pi i J_1'(ka) H_1^{(1)'}(ka)} \left(1 + \frac{\alpha}{k} \right)^{-1} \exp \left\{ \frac{i\alpha a}{\pi} \left[1 - 0.57721 + \ln\left(\frac{2\pi}{ka}\right) + i\frac{\pi}{2} \right] \right\} \\ \cdot \exp \left[\frac{-ika}{2} + \frac{i\alpha \gamma}{\pi} \ln\left(\frac{\alpha - \gamma}{k}\right) + p(\alpha) \right] \prod_{m=1}^{\infty} \left(1 + \frac{\alpha}{i\gamma_m} \right) e^{i\alpha a/m\pi}$$

where

$$\gamma'_m = \sqrt{(j'_m/a)^2 - k^2} = -i\sqrt{k^2 - (j'_m/a)^2}; \quad \gamma = \sqrt{\alpha^2 - k^2} \\ = -i\sqrt{k^2 - \alpha^2}$$

$$j'_m = \text{ordered zero of } J'_1(x)$$

$$p(\alpha) = \frac{1}{\pi} \int_0^\infty \left[1 - \frac{2}{\pi x} \frac{1 - \frac{1}{x^2}}{J_1'^2(x) + Y_1'^2(x)} \right] \ln \left[1 + \frac{\alpha a}{\sqrt{(ka)^2 - x^2}} \right] dx. \quad (4.17b)$$

The asymptotic behavior of $M_+(\alpha)$ is

$$M_+(\alpha) \sim \alpha^{-1/2} \quad (4.18)$$

as $|\alpha| \rightarrow \infty$ with $\text{Im } \alpha > 0$.

5. MAGNETIC FIELD AND DISTORTION PARAMETER

In the Fourier transform domain, the complete magnetic field is given below, for $\rho > a$

$$H_\rho(\rho, \phi, \alpha) \cong \sqrt{\frac{\epsilon}{\mu}} 2 \cos \phi \left[\frac{\alpha \kappa}{k} A(\alpha) H_1^{(1)'}(\kappa \rho) + \frac{i}{\rho} B(\alpha) H_1^{(1)}(\kappa \rho) \right] \quad (5.1)$$

$$H_\phi(\rho, \phi, \alpha) \cong \sqrt{\frac{\epsilon}{\mu}} 2i \sin \phi \left[\frac{i\alpha}{\kappa \rho} A(\alpha) H_1(\kappa \rho) - \kappa B(\alpha) H_1^{(1)'}(\kappa \rho) \right] \quad (5.2)$$

$$H_z(\rho, \phi, \alpha) \cong \sqrt{\frac{\epsilon}{\mu}} 2 \cos \phi \frac{i\kappa^2}{k} A(\alpha) H_n^{(1)}(\kappa \rho) \quad (5.3)$$

in which we have restored the ϕ -variation. For a field in the region $\rho < a$, we simply replace $A(\alpha)$ by $C(\alpha)$, $B(\alpha)$ by $D(\alpha)$, and the Hankel functions by Bessel functions in Equations (5.1) through (5.3). The explicit

solutions of A, B, C, and D are given in Equations (3.14) and (3.15) with $n = +1$.

To obtain the expressions of the magnetic field in the spatial domain, we take the inverse Fourier transform:

$$H_\rho(\rho, \phi, z) = \frac{\cos \phi}{i\pi k} \frac{2(ka)^2 M_+(k)}{N_+(k)} \int_C \frac{\alpha M_+(\alpha)}{k - \alpha} \left\{ \begin{array}{l} H_1^{(1)'}(\kappa\rho)/H_1^{(1)'}(\kappa a) \\ J_1'(\kappa\rho)/J_1'(\kappa a) \end{array} \right\} e^{-i\alpha z} d\alpha$$

$$+ \frac{i \cos \phi}{\pi \rho} \frac{ka L_+(k)}{N_+(k)} \int_C \frac{L_+(\alpha)}{(k^2 - \alpha^2)} \left\{ \begin{array}{l} H_1^{(1)}(\kappa\rho)/H_1^{(1)}(\kappa a) \\ J_1(\kappa\rho)/J_1(\kappa a) \end{array} \right\} e^{-i\alpha z} d\alpha$$

$$H_\phi(\rho, \phi, z) = \frac{i \sin \phi}{\pi k \rho} \frac{2(ka)^2 M_+(k)}{N_+(k)} \int_C \frac{\alpha M_+(\alpha)}{k - \alpha \sqrt{k^2 - \alpha^2}} \left\{ \begin{array}{l} H_1^{(1)}(\kappa\rho)/H_1^{(1)'}(\kappa a) \\ J_1(\kappa\rho)/J_1'(\kappa a) \end{array} \right\} e^{-i\alpha z} d\alpha$$

$$- \frac{i \sin \phi}{\pi} \frac{ka L_+(k)}{N_+(k)} \int_C \frac{L_+(\alpha)}{\sqrt{k^2 - \alpha^2}} \left\{ \begin{array}{l} H_1^{(1)'}(\kappa\rho)/H_1^{(1)}(\kappa a) \\ J_1'(\kappa\rho)/J_1(\kappa a) \end{array} \right\} e^{-i\alpha z} d\alpha$$

$$H_z(\rho, \phi, z) = \frac{\cos \phi}{\pi k} \frac{2(ka)^2 M_+(k)}{N_+(k)} \quad (5.6)$$

$$\times \int_C \frac{k + \alpha}{\sqrt{k^2 - \alpha^2}} M_+(\alpha) \left\{ \begin{array}{l} H_1^{(1)}(\kappa\rho)/H_1^{(1)'}(\kappa a) \\ J_1(\kappa\rho)/J_1'(\kappa a) \end{array} \right\} e^{-i\alpha z} d\alpha$$

$$\text{for } \left\{ \begin{array}{l} \rho > a \\ \rho < a \end{array} \right\}$$

in which the integration contour C is shown in Figure 2.

In the EMP study, a quantity of interest is the current on the outside surface of the hollow cylinder, which for $z < 0$ is given by

$$J_z(\phi, z) = H_\phi(\rho = a+) = F_z(z) \sin \phi \quad (5.7)$$

$$J_\phi(\phi, z) = -H_z(\rho = a+) = F_\phi(z) \cos \phi. \quad (5.8)$$

From Equations (5.5) and (5.6), the expressions for the surface currents can be easily written. For numerical computations, it is preferable to deform the integration path C in Figure 2 to a new path $(P_1 + P_2)$ around the branch cut in the upper-half α -plane (Figure 3). Note the relations:

$$\frac{H_1^{(1)}(\kappa a)}{\kappa H_1^{(1)' }(\kappa a)} \Big|_{P_1} - \frac{H_1^{(1)}(\kappa a)}{\kappa H_1^{(1)' }(\kappa a)} \Big|_{-P_2} = \frac{H_1^{(1)}(\kappa a)}{\kappa H_1^{(1)' }(\kappa a)} \Big|_{P_1} - \frac{H_1^{(1)}(-\kappa a)}{-\kappa H_1^{(1)' }(-\kappa a)} \Big|_{P_1} \quad (5.9)$$

$$= \frac{4}{i\pi\kappa^2 [J_1'^2(\kappa a) + Y_1'^2(\kappa a)]} \Big|_{P_1},$$

and

$$\frac{H_1^{(1)' }(\kappa a)}{\kappa H_1^{(1)}(\kappa a)} \Big|_{P_1} - \frac{H_1^{(1)' }(\kappa a)}{\kappa H_1^{(1)}(\kappa a)} \Big|_{-P_2} = \frac{4i}{\pi\kappa^2 [J_1^2(\kappa a) + Y_1^2(\kappa a)]}. \quad (5.10)$$

We may reduce the integrals for the surface current along the new path $(P_1 + P_2)$ to the following expressions:

$$F_z(z) = \frac{4}{\pi^2 N_+(k)} (g_1 + g_2), \quad -\infty < z < 0 \quad (5.11)$$

$$F_{\phi}(z) = \frac{8ika M_+(k)}{\pi^2 N_+(k)} (g_3 + g_4), \quad -\infty < z < 0 \quad (5.12)$$

in which

$$g_1(z) = \int_0^k \left[\frac{2\alpha}{k-\alpha} \frac{M_+(k) M_+(\alpha)}{G'(\sqrt{k^2 - \alpha^2} a)} + \frac{L_+(k) L_+(\alpha)}{G(\sqrt{k^2 - \alpha^2} a)} \right] \frac{ke^{-i\alpha z}}{k^2 - \alpha^2} d\alpha \quad (5.13)$$

$$g_2(\alpha) = \int_0^{\infty} \left[\frac{2\beta}{k-i\beta} \frac{M_+(k) M_+(i\beta)}{G'(\sqrt{k^2 + \beta^2} a)} - \frac{iL_+(k) L_+(i\beta)}{G(\sqrt{k^2 + \beta^2} a)} \right] \frac{ke^{\beta z}}{k^2 + \beta^2} d\beta \quad (5.14)$$

$$g_3 = \int_0^k \frac{M_+(\alpha) e^{-i\alpha z}}{(k-\alpha) G'(\sqrt{k^2 - \alpha^2} a)} d\alpha \quad (5.15)$$

$$g_4 = \int_0^{\infty} \frac{-i M_+(i\beta) e^{\beta z}}{(k-i\beta) G'(\sqrt{k^2 + \beta^2} a)} d\beta \quad (5.16)$$

$$G(x) = J_1^2(x) + Y_1^2(x) \quad (5.17)$$

$$G'(x) = J_1'^2(x) + Y_1'^2(x). \quad (5.18)$$

The advantage of deforming the integration path C to $(P_1 + P_2)$ may be seen from Equations (5.14) and (5.16). In these two infinite integrals, the integrands decay exponentially, and consequently they can be evaluated numerically without difficulty.

In addition to the current, another quantity of interest is the alteration of the incident magnetic field due to the presence of the semi-infinite cylinder (sensing boom). Let us introduce a magnetic field distortion

factor D such that

$$D(\rho, \phi, z) = \frac{H_x}{H_x^{(i)}} \quad (5.19)$$

which is the ratio of the scattered magnetic field H_x and the incident magnetic field. Then the measured field with meters supported by a sensing boom $(H_x + H_x^{(i)})$ is related to the undisturbed EMP field by the relation,

$$\text{EMP magnetic field} = \frac{\text{measured magnetic field}}{1 + D} \quad (5.20)$$

From the expressions in Equations (5.4) and (5.5), and the definition in Equation (5.7), it may be shown that

$$D(\rho, \phi, z) = \frac{(ka)^2 M_+(k) e^{ikz}}{N_+(k)} \int_C d_1(\rho, \phi, \alpha) \frac{\alpha}{k(k-\alpha)} \frac{H_1^{(1)'(\kappa a)}}{M_-(\alpha)} e^{-i\alpha z} d\alpha \quad (5.21)$$

$$- \frac{(ka) L_+(k) e^{ikz}}{2N_+(k)} \int_C d_2(\rho, \phi, \alpha) \frac{H_1^{(1)}(\kappa a)}{\kappa L_-(\alpha)} e^{-i\alpha z} d\alpha, \quad \rho < \alpha \text{ and } 0 < z < \infty$$

where d_1 and d_2 are the only functions depending on (ρ, ϕ) in the integrands and are given by

$$d_1(\rho, \phi, \alpha) = 2 \left[\frac{J_1(\sqrt{k^2 - \alpha^2} \rho)}{\sqrt{k^2 - \alpha^2} \rho} - J_2(\sqrt{k^2 - \alpha^2} a) \cos^2 \phi \right] \quad (5.22)$$

$$d_2(\rho, \phi, \alpha) = 2 \left[\frac{J_1(\sqrt{k^2 - \alpha^2} \rho)}{\sqrt{k^2 - \alpha^2} \rho} - J_2(\sqrt{k^2 - \alpha^2} a) \sin^2 \phi \right]. \quad (5.23)$$

For numerical evaluation, we will deform the integration path C in Equation (5.21) into a new path $P_3 + P_4$ in the lower-half α -plane (Figure 3), and obtain the result:

$$D(\rho, \phi, z) = \frac{k a e^{i k z}}{N_+(k)} [g_5 + g_6], \quad \rho < a \text{ and } 0 < z < \infty \quad (5.24)$$

in which

$$g_5(\rho, \phi, z) = - \int_0^k [2ka \frac{\alpha M_+(k)}{k(k+\alpha)} \frac{J_1'(\sqrt{k^2 - \alpha^2} a)}{M_+(\alpha)} d_1(\rho, \phi, \alpha) + \quad (5.25)$$

$$+ L_+(k) \frac{J_1(\sqrt{k^2 - \alpha^2} a)}{\sqrt{k^2 - \alpha^2} L_+(\alpha)} d_2(\rho, \phi, \alpha)] e^{i \alpha z} d\alpha$$

$$g_6(\rho, \phi, z) = \int_0^\infty [2ka \frac{-\beta M_+(k)}{k(k+i\beta)} \frac{J_1'(\sqrt{k^2 + \beta^2} a)}{M_+(i\beta)} d_1(\rho, \phi, i\beta) + \quad (5.26)$$

$$+ i L_+(k) \frac{J_1(\sqrt{k^2 + \beta^2} a)}{\sqrt{k^2 + \beta^2} L_+(i\beta)} d_2(\rho, \phi, i\beta)] e^{-\beta z} d\beta.$$

Again the integrand in the infinite integral in Equation (5.26) decays exponentially. In many practical applications, we are often interested in the distortion on the axis of the cylinder:

$$D_0(z) = D(\rho, \phi, z) \Big|_{\rho=0} \quad (5.27)$$

which is a function of z only. For computation of $D_0(z)$, we simply set

$d_1 = d_2 = 1$ in Equations (5.25) and (5.26).

6. LOW-FREQUENCY APPROXIMATION

In this section, we will derive a set of approximate formulas for the scattered field when the frequency is low. Explicitly, we assume that

$$ka \ll 1, \quad \text{and} \quad |a/z| \ll 1 \quad (6.1)$$

in which the second condition is introduced in order to avoid the evaluation of the field in the so-called "boundary layer" (regions where kz is also small so that $|a/z|$ may assume a fixed number). In the boundary layer, the scattered field varies rapidly and it is very difficult to obtain an analytical expression for the scattered field there.

We will now expand the scattered field in an ascending power series of (ka) , and drop all terms of $O(k^2 a^2)$ or higher. First let us consider $L_+(\alpha)$ and $M_+(\alpha)$. As will become clear later, our solution under assumption (6.1) depends mainly on $L_+(\alpha)$ and $M_+(\alpha)$ with α in the range $\alpha \sim k$ or less. Within this range we may approximate $L(\alpha)$ in Equation (4.1) and $M(\alpha)$ in Equation (4.2) by

$$L(\alpha) \sim 1 - \frac{(k^2 - \alpha^2)a^2}{2} \ln \frac{\sqrt{k^2 - \alpha^2} a}{2} \quad (6.2)$$

$$M(\alpha) \sim \left[1 + \frac{(k^2 - \alpha^2)a^2}{2} \ln \frac{\sqrt{k^2 - \alpha^2} a}{2} \right] \frac{-1}{a^2(k^2 - \alpha^2)} \quad (6.3)$$

where the terms of $O(k^2 a^2)$ or higher have been dropped. The factorization of Equations (6.2) and (6.3) can be obtained by inspection with the results:

$$L_+(\alpha) \approx 1 - \frac{(k^2 - \alpha^2)a^2}{2} \ln \sqrt{\frac{(k + \alpha)a}{2}} \quad (6.4)$$

$$M_+(\alpha) \approx \frac{i}{(k + \alpha)a} \left[1 + \frac{(k^2 - \alpha^2)a^2}{2} \ln \sqrt{\frac{(k + \alpha)a}{2}} \right] \quad (6.5)$$

$$\text{for } k^2 a^2, \quad |\alpha|^2 a^2 \ll 1.$$

Next, we will use the results in Equations (6.4) and (6.5) in Equation (5.24) for the evaluation of the distortion parameter $D(\rho, \phi, z)$. When the terms of $O(k^2 a^2)$ or higher are dropped, the integral in Equation (5.25) becomes

$$g_5 \approx -\frac{a}{2} \int_0^k \left(\frac{\alpha}{k} + 1\right) e^{i\alpha z} d\alpha - \frac{a^3}{2} \int_0^k \frac{(k - \alpha)(k^2 - \alpha^2)}{4k} \left[\ln \frac{(k + \alpha)a}{2} \right] e^{i\alpha z} d\alpha. \quad (6.6)$$

The first integral in Equation (6.6) can be evaluated easily, while the second one can be approximated by

$$\begin{aligned}
 & -\frac{a^3}{8} \ln \frac{ka}{2} \int_0^k (\alpha - k)^2 e^{i\alpha z} d\alpha \\
 & = \frac{1}{8i} \left(\frac{a}{z}\right)^3 \left(\ln \frac{ka}{2}\right) [2e^{ikz} + (k^2 z^2 - 2ikz - 2)].
 \end{aligned} \tag{6.7}$$

Thus, we have

$$\begin{aligned}
 g_5 & \sim i \left(\frac{a}{z}\right) \left[1 - \frac{1}{2ikz} - \frac{1}{4} \left(\frac{a}{z}\right)^2 \ln \frac{ka}{2}\right] e^{ikz} \\
 & - \frac{i}{2} \left(\frac{a}{z}\right) \left[1 - \frac{1}{ikz} + \frac{1}{4} \left(\frac{a}{z}\right)^2 \left(\ln \frac{ka}{2}\right) (k^2 z^2 - 2ikz - 2)\right].
 \end{aligned} \tag{6.8}$$

For the integral g_6 in Equation (5.26), we note that the exponentially decaying nature of the integrand allows the use of Equations (6.4) and (6.5). Then it may be evaluated in a similar fashion as g_5 , and its result is

$$g_6 \sim \frac{i}{2} \left(\frac{a}{z}\right) \left[1 - \frac{1}{ikz} + \frac{1}{4} \left(\frac{a}{z}\right)^2 \left(\ln \frac{ka}{2}\right) (k^2 z^2 - 2ikz - 2)\right]. \tag{6.9}$$

Recalling the definition of $N_+(k)$ in Equation (3.15) and the use of Equations (6.4) and (6.5) results in

$$N_+(k) \sim -2. \tag{6.10}$$

Substitution of Equations (6.7) through (6.10) in Equation (5.24) gives the desired result,

$$D_o(z) \approx \frac{ka}{2i} \left(\frac{a}{z}\right) \left[1 - \frac{1}{ikz} - \frac{1}{4}\left(\frac{a}{z}\right)^2 \ln \frac{ka}{2}\right] e^{i2kz} \quad (6.11)$$

which is valid under the conditions in Equation (6.1).

Similar procedures can be applied to the approximate evaluation of the current in Equations (5.7) through (5.18). The results are

$$J_z \approx \frac{\sin \phi}{2} \left(\frac{a}{z}\right)^2 \left[1 + i \frac{3}{2}\left(\frac{a}{z}\right) (ka \ln \frac{ka}{2})\right] e^{-ikz} \quad (6.12)$$

$$J_\phi \approx \cos \phi \left(\frac{a}{z}\right)^3 \left[1 + ikz - \frac{3}{4}(ka)^2 (\ln \frac{ka}{2})\right] e^{-ikz} \quad (6.13)$$

We will estimate the accuracy of Equations (6.11) through (6.13) by comparing them with results obtained by numerical integrations in Section 7.

7. NUMERICAL RESULTS AND DISCUSSION

In the previous section, the scattered field due to a normally incident plane wave has been obtained, and is expressed in terms of inverse Fourier integrals. Details of the numerical computation, particularly the convergence of the various integrals, are discussed in the Appendix. In this section, we will only present the numerical data relevant to the physical problem under consideration.

(a) Distortion parameter as a function of ka

The magnetic field distortion parameter as defined in Equation (5.19) is given by

$$D(\rho, \phi, z) = \frac{H_x(\rho, \phi, z)}{H_x^{(i)}(z)} = e^{ikz} H_x(\rho, \phi, z), \quad z > 0 \quad (7.1)$$

which is a measurement of the amount of distortion due to the presence of the cylindrical boom. First let us concentrate on the distortion along the

axis, that is $D_0(z) = D(\rho = 0, z)$, as a function of the radius of the cylinder ka . The numerical results are presented in Figure 4. A dominant feature of the curve is that D_0 assumes maximum values at the zeros of $J_1'(ka)$, namely at

$$ka = 1.841, 5.331, \dots$$

which are the resonant values for the TE_{1m} modes in the interior of the cylindrical tube. These values are also the related zeros of $M_+(\alpha)$ as given in (4.17a). The zeros of $J_1(ka)$ or $L_+(\alpha)$ at $ka = (\alpha/k) = 3.831, \dots$, etc., play a secondary role in the determination of D_0 . In general, $|D_0|$ decreases as ka increases. This is due to the fact that the larger the cylinder, the easier the wave can be transmitted into the tube. In EMP applications, we generally are interested in cases with $0 < ka < 1.841$.^{*} In this range, $|D_0|$ increases with ka . Thus, for a given boom (fixed a), the high-frequency components in the EMP are distorted more than the low-frequency components for axial incidence. Figure 4 presents the distortion on the axis $\rho = 0$ only. In the neighborhood of the axis, the field varies slowly as indicated in Table 1. Thus, in the following discussion, we will concentrate on the field on the axis.

(b) Distortion parameter as a function of kz

Such computations are presented in Figure 5 for several different values of ka . Note that the distortion assumes its maximum value at a distance $(kz)_{\max}$ and then decreases as (kz) increases. For $ka < 1.5$, $(kz)_{\max}$ is roughly given by the simple equation

$$(kz)_{\max} \approx 0.46(ka) + 0.2, \text{ for } \rho = 0. \quad (7.2)$$

^{*}For example, with a sensor boom 6 inches in diameter, we have $ka = 0.16$ at a frequency of 100 Mc/s.

TABLE 1

ABSOLUTE VALUE OF $D(\rho, \phi, z)$ AT $\phi = 0$ PLANE

kz	ka	$\rho = 0$	$\rho = 0.5a$	$\rho = a$
1.2	0.2	0.0179	0.0178	0.0175
	0.5	0.1171	0.1142	0.1060
	1	0.4676	0.4572	0.4026
1.8	0.2	0.0118	0.0117	0.0116
	0.5	0.0805	0.0791	0.0749
	1	0.3700	0.3522	0.2798

Thus, to avoid large distortion, for axial incidence the measurement instruments placed at the end of the sensor boom should avoid the neighborhood of the point described in Equation (7.2).

The phase variation of D_0 is presented in Figure 5b. An interesting feature is that for $z \gg a$, the phase varies almost linearly with z .

* Approximately, D_0 can be expressed in the form

$$D_0(z) = |D_0(z)| e^{-i(k+\beta)z} e^{i\psi}$$

where ψ is a constant, independent of z . Recalling the definition in Equation (7.1), the relation in Equation (7.3) implies that the scattered field $H_x(\rho = 0, z)$ has a phase variation of the type

$$H_x(\rho = 0, z) = |H_x(\rho = 0, z)| e^{-i\beta z} e^{i\psi}.$$

Thus, ψ may be regarded as the phase delay introduced at the reflecting plane at $z = 0$ for the scattered field, and β is the wave number of the reflected traveling wave. From the data in Figure 5b, the values of (ψ, β) can be approximately determined and the results are tabulated in Table 2. It is noted that $(\beta/k) \approx 0.98$ for all the cases considered in Figure 6. The data presented in Figure 5a is reflected in Figure 6 as a function of (z/a) . It is clear, that maximum distortion occurs around $z = 0.5a$, as indicated in (7.2).

(c) Error in EMP measurement

In EMP studies, a problem of interest is the percentage of error in the measurement of EMP field introduced by the boom. When the incident EMP is approximately single frequency, we are only concerned with the error in the magnitude of the field, and not in the phase. In such a situation, we may define an error by the definition

$$\begin{aligned} e(z) &= \frac{(\text{mag. of total field}) - (\text{mag. of incident field})}{\text{mag. of incident field}} \times 100 \% \\ &= \frac{|H^{(\text{total})}(\rho = 0, z)| - |H^{(i)}(\rho = 0, z)|}{|H^{(i)}(\rho = 0, z)|} \times 100 \% \\ &= [|1 + D_o(z)| - 1] \times 100 \%. \end{aligned} \quad (7.5)$$

Some typical computations of $e(z)$ are given in Figure 7. For small ka , e.g., $ka \lesssim 0.5$, the error is large at the immediate neighborhood of the end of the boom, and is zero roughly at

$$kz \approx 1.4 + \frac{n\pi}{2}, \quad n = 0, 1, 2, 3, \dots, \text{ and } \rho = 0. \quad (7.6)$$

The formula in Equation (7.6) can be derived from Equation (7.5) by

TABLE 2

VALUES OF PHASE DELAY AND WAVE NUMBER FOR SCATTERED MAGNETIC FIELD ON AXIS

ka	ψ	β/k
0.1	79°	0.98
0.2	79°	0.98
0.3	79°	0.98
0.5	113°	0.98
1.0	309°	0.98
1.5	355°	0.98
1.841	67°	0.98
2.0	77°	0.98

using the analytical formula of $D_o(z)$ given in Section 6. Thus, an important observation can be made: When the incident EMP is predominantly single-frequency, and that frequency is low enough so that $ka \lesssim 0.5$, the error in measurement can be minimized by placing measurement instruments at locations described in Equation (7.6). As a numerical example, at $f = 200$ Mc/s and with a boom of 6 inch diameter, the error can be as large as 11 per cent when the instruments are placed at $z = 3$ inches. However, this error can be reduced to zero when the instruments are placed at $z = 13$ inches. It should be emphasized that this conclusion is reached only under the assumption that the EMP is predominantly single-frequency. Otherwise, the error can be reduced only when $|D_o|$, as shown in Figure 6a, is small for a band of frequencies of interest.

(d) Circumferential current $J_\phi(\phi, z)$ as a function of (kz)

This current on the outer surface of the cylinder is given by formulas (5.8) and (5.12). These formulas show that the current has an explicit dependence on ϕ of the form $\cos \phi$. Therefore, division of the current by $\cos \phi$ renders it independent of ϕ . Variation of the magnitude and phase of $J_\phi/\cos \phi$ with respect to kz and for several values of ka is given in Figures 8a and 8b, respectively. Again, the current is in the form of a traveling wave with a propagation constant β slightly less than k .

(e) Axial current $J_z(\phi, z)$ as a function of kz

The axial current on the surface of the semi-infinite cylinder is given

by formulas (5.7) and (5.11). The dependence of this current on ϕ is of the form $\sin \phi$. The magnitude and phase of $J_z(\phi, z)/\sin \phi$ as a function of kz and for different values of ka are given in Figures 9a and 9b, respectively.

(f) Accuracy of the approximate formulas

In Section 6, simple approximate formulas are derived for the scattered field and related quantities. These formulas are valid under the assumptions that

$$ka \ll 1 \text{ and } kz \gg 1. \quad (7.7)$$

To test their accuracy, we present in Figures 10 and 11, a comparison of the results for $H_x^{(\text{total})}$ and J_ϕ , respectively, as obtained by numerical integration and the approximate formulas in Section 5. Generally speaking the approximate formulas are reasonably accurate when

$$ka \lesssim 0.5 \text{ and } kz > ka. \quad (7.8)$$

More detailed comparisons are given in the Appendix.

8. CONCLUSION

In this paper, we have obtained the near field solution for scattering by a semi-infinite tube due to a normally incident plane wave. The numerical computation is facilitated by using a new factorization formula for the Wiener-Hopf kernel as appeared in the solution of the problem (Section 4). For low frequencies, approximate formulas for the scattered field and the related quantities given by simple analytic expressions are obtained (Section 6), and they are found to be reasonably accurate for $ka \lesssim 0.5$ and $kz > ka$.

The results obtained in this theoretical problem are used to evaluate the field distortion due to the presence of the sensor boom in the EMP measurement

(Section 7). It is found that the distortion problem is particularly severe at the interior resonance frequencies for the TE mode of the sensor tube, namely, at $ka = 1.841, 5.331, \dots$. For example, at $ka = 1.841$ and with the measurement instruments placed at $\rho = 0$ and $kz = 2.1$, the error in measurement can be as large as 100 per cent!

For many practical cases, the high-frequency components in the EMP field are probably small enough such that $0 < ka < 1$ (for a boom of 6 inch diameter, this means that no significant field component exists beyond 1,000 Mc). Under this assumption, guidelines for reducing measurement error are listed below:

(i) For a given z (the distance between the instrument and the end of the boom), the distortion is proportional to the radius of the boom a (Figure 6a). Thus, a should be made as small as practical.

(ii) The maximum distortion occurs at a distance of about one half of the radius away from the end of the boom, and becomes insignificant at about five radii away (less than 20 per cent for $ka < 1$, see Figure 6c). Thus, the measuring instruments should not be placed very close to the end. It should be emphasized that the above two guidelines are based on the observation of axial incidence. Further study is needed to ascertain whether they continue to be valid for oblique incidence.

APPENDIX. DETAILS OF NUMERICAL COMPUTATIONS

In this section, the problem formulated in Sections 2 through 6 will be numerically solved; that is, the values of the scattered magnetic field, distortion parameters and currents on the surface of a semi-infinitely long hollow cylinder, due to an axially incident plane wave, will be calculated.

The first and a crucial step in the evaluation of field and related quantities is the numerical evaluation of $L_+(\alpha)$ and $M_+(\alpha)$.

(a) Evaluation of $L_+(\alpha)$:

$L_+(\alpha)$ has been formulated in Section 4 and is given by (4.16). Here it is rewritten as

$$L_+(\alpha) = L_+(\alpha/k) = e^{\chi(\alpha/k)} L_+^{(1)}(\alpha/k) L_+^{(2)}(\alpha/k) \quad (\text{A.1})$$

in which

$$\chi(\alpha/k) = \frac{i}{\pi} (\alpha/k) (ka) [0.42279 + \ln(2\pi/ka) + i \frac{\pi}{2}]; \quad (\text{A.2})$$

and

$$L_+^{(1)}(\alpha/k) = \sqrt{\pi i J_1(ka)} \prod_{m=1}^{\infty} \left(1 + \frac{(\alpha/k)}{i(\gamma_m/k)}\right) e^{i(\alpha/k)(ka)/m\pi}, \quad (\text{A.3})$$

in which

$$\left(\frac{\gamma_m}{k}\right) = \sqrt{\left(\frac{j_m}{ka}\right)^2 - 1} = -i\sqrt{1 - \left(\frac{j_m}{ka}\right)^2}, \quad (\text{A.4})$$

j_m = ordered zero of $J_1(x)$.

Also the last factor in (A.1) is given as

$$L_+^{(2)}(\alpha/k) = \sqrt{H_1^{(1)}(ka)} \exp\left[-\frac{i(ka)}{2} + \frac{i(ka)(\gamma/k)}{\pi} \ln\left(\frac{\alpha}{k} - \frac{\gamma}{k}\right) + q(\alpha)\right], \quad (\text{A.5})$$

in which

$$\left(\frac{Y}{k}\right) = \sqrt{(\alpha/k)^2 - 1} = -i\sqrt{1 - (\alpha/k)^2}, \quad (\text{A.6})$$

and

$$q(\alpha/k) = \frac{1}{\pi} \int_0^{\infty} \left(1 - \frac{2}{\pi x} \frac{1}{J_1^2(x) + Y_1^2(x)} \ln\left(1 + \frac{(ka)(\alpha/k)}{\sqrt{(ka)^2 - x^2}}\right)\right) dx, \quad (\text{A.7})$$

noting that

$$\sqrt{(ka)^2 - x^2} = i\sqrt{x^2 - (ka)^2} \text{ for } x > ka.$$

$L_+(\alpha/k)$ has been previously calculated for certain values of (ka) and (α/k) , albeit based on different formulations, by Jones⁷ and Matsui.¹⁶

Therefore, a base exists for comparison in calculating $L_+(\alpha/k)$.

Furthermore, the low frequency approximation for $L_+(\alpha/k)$ is given by (6.4) as

$$L_+(\alpha/k) \approx 1 - \frac{(ka)^2}{4} \left[1 - \left(\frac{\alpha}{k}\right)^2\right] \ln\left[ka\left(1 + \frac{\alpha}{k}\right)\right] \quad (\text{A.8})$$

for $k^2 a^2, |\alpha^2| a^2 \ll 1,$

which may be used to check the correctness of numerical computation of the general formula.

There are two factors in the computation of $L_+(\alpha/k)$ which require special attention. The first one is the evaluation of the infinite product in (A.3), i.e.,

$$\lim_{m \rightarrow \infty} \prod_{m=1}^M \left(1 - \frac{(\alpha/k)}{i(\gamma_m/k)}\right) e^{i(\alpha/k)(ka)/m\pi}. \quad (\text{A.9})$$

Fortunately, this product is convergent and a maximum value for M may be chosen so as to render it numerically computable. The first few values of j_m are found in most of the books on mathematical tables.¹⁵ For large values of m

the following asymptotic formula is used

$$j_m = \beta - \frac{3}{8\beta}; \quad \beta = (m + \frac{1}{4})\pi \text{ for } m \rightarrow \infty. \quad (\text{A.10})$$

The product (A.9) has been calculated for several values of M and for $\alpha/k = 1$; the results are given in Table 3. It is observed that as ka increases, the convergence of the product is slower; but in any case the increase from M = 200 to M = 300 is far below 1 per cent. Throughout the rest of the numerical calculations, the value of M = 300 is used.

The second consideration is the method of evaluation of the Cauchy principal value in the integral (A.7). Apparently, the integrand in (A.7) becomes infinitely large for the value of $x = ka$. In order to investigate the behavior of the integral (A.7), around the point $x = ka$, the following integral is considered

$$I = \lim_{\epsilon_0 \rightarrow 0} \int_{ka(1-\epsilon_0)}^{ka(1-\epsilon_0)} + \int_{ka(1+\epsilon_0)}^{ka(1+\epsilon_0)} \frac{1}{\pi} \left(1 - \frac{2}{\pi x} \frac{1}{J_1^2(x) + Y_1^2(x)} \ln \left(1 + \frac{(ka)(\alpha/k)}{\sqrt{(ka)^2 - x^2}} \right) \right) dx \quad (\text{A.11})$$

in which $\epsilon \ll 1$. Considering the very small interval of integration and using some approximations due to very small value of ϵ , and after some lengthy manipulation the value of integral (A.11) is evaluated as

$$I \approx \frac{1}{\pi} \left(1 - \frac{2}{\pi(ka)} \frac{1}{J_1^2(ka) + Y_1^2(ka)} \right) (ka) \epsilon \left[\ln \left(\frac{1}{2\epsilon} \right) + 2 \ln \left(\frac{\alpha}{k} \right) + \frac{3}{2} - j \frac{\pi}{2} \right]. \quad (\text{A.12})$$

It is observed from (A.12) that the integral (A.11) is limited and approaches zero as $\epsilon \rightarrow 0$. Therefore, finally $q(\alpha/k)$ in (A.7) can be written as

$$q(\alpha/k) = \int_0^{ka(1-\epsilon)} (\dots) dx + I + \lim_{x_{\max} \rightarrow \infty} \int_{ka(1+\epsilon)}^{x_{\max}} (\dots) dx \quad (\text{A.13})$$

TABLE 3

VALUE OF THE PRODUCT (A.9) FOR DIFFERENT VALUES OF M

ka \ M	1	2	3	4	5
10	1.05646+i0.09731	1.27618+i0.20284	1.99402+i0.29628	1.37763+i6.71580	-0.46300+i5.24035
50	1.05980+i0.10387	1.29282+i0.22082	2.05638+i0.34135	1.30484+i7.15848	-0.66065+i5.73690
100	1.06024+i0.10474	1.29504+i0.22327	2.06477+i0.34766	1.29309+i7.21945	-0.69094+i5.80583
150	1.06039+i0.10504	1.29578+i0.22410	2.06760+i0.34978	1.28902+i7.24009	-0.70137+i5.82919
200	1.06047+i0.10519	1.29616+i0.22451	2.06987+i0.35087	1.28695+i7.25047	-0.70664+i5.84094
250	1.06051+i0.10528	1.29638+i0.22476	2.06987+i0.35152	1.28571+i7.25671	-0.70982+i5.84801
300	1.06054+i0.10534	1.29653+i0.22493	2.07044+i0.35196	1.28487+i7.26088	-0.71195+i5.85270

$$\alpha/k = 1$$

in which the integrands are the same as in (A.7).

In order for the second integral to be numerically tractable, we have to choose a maximum value x_m beyond which the value of the integral can be ignored. To this end we should investigate the asymptotic behavior of the integrand for $x \gg ka$. This is done and leads to the following results

$$\left(1 - \frac{2}{\pi x} \frac{1}{J_1^2(x) + Y_1^2(x)}\right) \xrightarrow{x \rightarrow \infty} \frac{3}{8} \frac{1}{x^2} \quad (\text{A.14})$$

$$\ln\left(1 + \frac{(\alpha/k) \left(\frac{ka}{x}\right)}{i \sqrt{1 - \left(\frac{ka}{x}\right)^2}}\right) \xrightarrow{\substack{\frac{ka}{x} \ll 1 \\ \left(\frac{ka}{x}\right) \left(\frac{\alpha}{k}\right) \ll 1}} \begin{cases} \left(\frac{ka}{x}\right) \xi(\alpha/k) \left[\frac{1}{2} \left(\frac{ka}{x}\right) \xi(\alpha/k) - i\right] & \text{for } \alpha/k \text{ real} \\ \left(\frac{ka}{x}\right) \xi|\alpha/k| & \text{for } (\alpha/k) \text{ pure imaginary} \end{cases}$$

in which

$$\xi = \left[1 + \frac{1}{2} \left(\frac{ka}{x}\right)^2\right]^{1/2} \approx 1, \text{ for } \frac{ka}{x} \ll 1.$$

It is apparent that for very large values of x , the second integrand in (A.13), with regard to (A.14) and (A.15), is of the order $(1/x^3)$ and, therefore, the integral has a remainder of the order $(1/x_{\max}^2)$. For very small values of x the first integrand in (A.13) can be approximated and leads to

$$\frac{1}{\pi} \left(1 - \frac{2}{\pi x} \frac{1}{J_1^2(x) + Y_1^2(x)}\right) \ln\left(1 + \frac{(ka)(\alpha/k)}{\sqrt{(ka)^2 - x^2}}\right) \xrightarrow{x \rightarrow 0} \frac{1}{\pi} \left(1 - \frac{\pi}{2} x\right) \ln[1 + (\alpha/k)] \quad (\text{A.16})$$

with regard to the above formulas and also numerical calculation of the integrand it can be said that for constant values of (α/k) and (ka) , the absolute value of the integrand in (A.7) starts from a certain value for $x = 0$,

and decreases, reaches a minimum with respect to x and then goes up to infinity for $x = ka$, then decreases rapidly and eventually goes to zero as $(1/x^3)$, (see Figure 12). Due to this behavior of the integrand of (A.7), it can be numerically calculated in the form of (A.13).

To evaluate the integral by computer, two integration methods have been considered tentatively. One is based on the trapezoidal rule in connection with Romberg's principle, which calculates the integral to any desired degree of accuracy. This method takes into account the end points. In the second method, evaluation is done by means of a 16-point Gauss quadrature formula which integrates exactly polynomials up to degree 31 and without considering the end points of the integral. Subroutines for these methods are obtained from IBM-SSP. Using the trapezoidal method for evaluation of (A.7) we have to make use of (A.13), but in the Gaussian method we could eliminate I and perform two integrations from 0 to ka and from ka to x_{\max} . Of course, in the latter case, also Equation (A.13) could be used; however, as will be shown, the results are not much different. Table 4 shows the resultant value of $L_+(\alpha/k)$ for several different forms of integration of (A.7) and as calculated by Matsui¹⁶ and Jones.⁷ As is observed, the difference in the results due to different methods is much less than 1 per cent. Also, it must be noticed that the trapezoidal method takes longer than the Gaussian method, depending on the desired accuracy. Therefore, in the rest of the calculations, only the Gaussian method is considered. Furthermore, it is seen that the difference between the results obtained by the Gaussian method, using the middle step, involving I , and the one not using it, is also much less than 1 per cent.

In order to better appreciate the extent of the influence of I as

TABLE 4

COMPARISON OF VALUES OF $L_+(\alpha/k)$ CALCULATED BY SEVERAL DIFFERENT METHODS

$ka = 1., \alpha/k = 1., M = 300$	$L_+(\alpha/k)$
$q(\alpha/k) = \int_0^{ka(1-\epsilon)} + \int_{ka(1+\epsilon)}^{10.}$ Trapezoidal method EPS = 10^{-2} Upper bound of absolute error in integration, $\epsilon = 10^{-5}, I \approx 0$	$0.72278 + i0.42127$
$q(\alpha/k) = \int_0^{ka} + \int_{ka}^{10.}$ 16-point Gaussian method	$0.71957 + i0.41949$
$q(\alpha/k) = \int_0^{ka} + \int_{ka}^{4.+ka}$ 16-point Gaussian method $= \frac{1}{\pi} (0.45986 - i0.14314)$	$0.71904 + i0.42084$
$q(\alpha/k) = \int_0^{ka(1-\epsilon)} + I + \int_{ka(1+\epsilon)}^{4.+ka}$ 16-point Gaussian method $= \frac{1}{\pi} (0.46174 - i0.14340)$ $\epsilon = 0.01$	$0.71950 + i0.42103$
Calculated by Jones ⁷	$0.7206 + i0.4235$
Calculated by Matsui ¹⁶	$0.7205 + i0.4196$

given by (A.11) or approximated by (A.12) on the final result of $q(\alpha/k)$, we proceed as follows. First we consider the value of I with $\epsilon = 0.01$, as calculated by numerical integration from (A.11) using a 16-point Gaussian quadrature method and compare the result with the approximate result of (A.12), as given in Table 5. It may be observed that the two results are very close; this indicates the correctness of approximation (A.12). Therefore, from this stage onward the value of I is calculated from (A.12) only. Second, the value of $q(\alpha/k)$ and its components are computed by Equation (A.13), using (A.12), with $\epsilon = 0.01$ and for several values of (α/k) and (ka) . Then the resultant values are compared with those obtained by $\epsilon = 0$ (that is, $I = 0$), and with two integrations from 0 to ka and from ka to x_{\max} , using the Gaussian method. Moreover, in order to see the insignificance of the remainder of the integral (A.13) for $x > x_{\max}$, the value of this integral from x_{\max} to $2x_{\max}$ is also calculated. In Table 5 a numerical account is given.

As a result of the above discussion and in view of the results of Tables 5 and 6, the evaluation of $q(\alpha/k)$, as given by Equation (A.7) is done according to Equation (A.13) with $\epsilon = 0$, $I = 0$, and using a 16-point Gaussian method of integration. Upon close study of the variation of the integrand in Equation (A.7), it is revealed that although the integrand decreases rapidly after $x = ka$, however, it assumes larger values for larger values of ka . Therefore, as a reasonable approximation we choose

$$x_{\max} = \text{constant} + ka = 4 + ka. \quad (\text{A.17})$$

Although this choice of x_{\max} seems rather arbitrary, it has been chosen on the basis of some numerical consideration. For values of $ka \lesssim 6$ we could choose

$$x_{\max} = 10,$$

TABLE 5

THE VALUE OF $q(\alpha/k)$ AND ITS COMPONENTS FOR DIFFERENT METHODS AND SEVERAL VALUES OF (ka) , (α/k)

α/k	ka	ϵ	$\pi \cdot \int_0^{ka(1-\epsilon)}$	$\pi \cdot I$	$\pi \cdot \int_{ka(1+\epsilon)}^{x_{\max}}$	$\pi \cdot q(\alpha/k)$	$\pi \cdot \int_{x_{\max}}^{2x_{\max}}$
1.	0.2	0.0		—		0.211605-10.18810	2.8×10^{-5} - 11.5×10^{-3}
		0.01	0.14216	$(0.00713-i0.00210)^{\dagger}$ $(0.00771-i0.00224)^{*}$	0.06388-i0.1861	0.21375-10.18837	
	1.	0.0		—		0.45986-10.14314	4.3×10^{-4} - 15.5×10^{-3}
		0.01	0.38252	$(0.01042-i0.00305)^{\dagger}$ $(0.01126-i0.00327)^{*}$	0.06951-i0.14013	0.46173-10.14340	
	3.	0.0		—		0.52789-10.05535	1.5×10^{-3} - 18.6×10^{-3}
		0.01	0.49178	$(0.00556-i0.00163)^{\dagger}$ $(0.00602-i0.00175)^{*}$	0.03083-i0.05372	0.52863-10.05549	
	7.	0.0		—		0.53872-10.01896	2.3×10^{-3} - 18.5×10^{-3}
		0.01	0.52396	$(0.00261-i7.6 \times 10^{-4})^{\dagger}$ $(0.00283-i8.2 \times 10^{-4})^*$	0.01224-i0.01819	0.53903-10.01916	

† Computed from (11), with $\epsilon = 0.01$ and using the 16-point Gaussian quadratic method.

* Computed from (12)

TABLE 5 -- CONTINUED

α/k	ka	ϵ	$\pi \cdot \int_0^{ka(1-\epsilon)}$	$\pi \cdot I$	$\pi \cdot \int_{ka(1+\epsilon)}^{x_{\max}}$	$\pi \cdot q(\alpha/k)$	$\pi \cdot \int_{x_{\max}}^{2x_{\max}}$
0.2	0.0			—		0.71849-i0.47543	$6.9 \times 10^{-4} - i 17.6 \times 10^{-3}$
	0.01	0.33990		(0.01160-i0.00221) [†] (0.01229-i0.00224) [*]	0.36859-i0.47325	0.72075+i0.47548	
1.	0.0			—		1.94908-i0.27816	$8.3 \times 10^{-3} - i 0.02339$
	0.01	0.93896		(0.01696-i0.00321) [†] (0.01796-i0.00327) [*]	0.29419-i0.27496	1.25112-i0.27823	
3.	0.0			—		1.36061-i0.09136	0.01779-i0.02707
	0.01	1.23829		(0.00906-i0.00171) [†] (0.00959-i0.00175) [*]	0.11355-i0.08965	1.36144-i0.09140	
7.	0.0			—		1.37956-i0.02743	0.01796-i0.02044
	0.01	1.33697		(0.00426-i8.0x10 ⁻⁴) [†] (0.00451-i8.2x10 ⁻⁴) [*]	0.03842-i0.02663	1.37990-i0.02745	

† Computed from (11), with $\epsilon = 0.01$ and using the 16-point Gaussian quadratic method.

* Computed from (12).

TABLE 5 — CONTINUED

α/k	ka	ϵ	$\pi \cdot \int_0^{ka(1-\epsilon)}$	$\pi \cdot I$	$\pi \cdot \int_{ka(1+\epsilon)}^{x_{\max}}$	$\pi \cdot q(\alpha/k)$	$\pi \cdot \int_{x_{\max}}^{2x_{\max}}$
2i	0.2	0.0		—		0.46560-10.20258	2.95×10^{-3}
		0.01	0.17354+i0.20040	$(9.03+i2.17) \times 10^{-3} \dagger$ $(9.68+i2.24) \times 10^{-3} *$	0.28453	0.46775+i0.20264	
	1.	0.0		—		0.67985+i0.56646	9.6×10^{-3}
		0.01	0.46029+i0.56327	$(0.01320+i3.19 \times 10^{-3}) \dagger$ $(0.01415+i3.27 \times 10^{-3}) *$	0.20738	0.68182+i0.56654	
	3.	0.0		—		0.66762+i0.75599	0.01364
		0.01	0.58229+i0.75428	$(7.05+i1.71) \times 10^{-3} \dagger$ $(7.56+i1.75) \times 10^{-3} *$	0.07857	0.66841+i0.75603	
	7.	0.0		—		0.64443+i0.82129	0.01250
		0.01	0.6145+i0.82049	$(3.3 \times 10^{-3} + i8.0 \times 10^{-4}) \dagger$ $(3.55 \times 10^{-3} + i8.2 \times 10^{-4}) *$	0.02671	0.64476+i0.82131	

† Computed from (11), with $\epsilon = 0.01$ and using 16-point Gaussian quadratic method.

* Computed from (12).

which leads to almost the same results as (A.17).

For comparison, sample values of $L_+(\alpha/k)$ as calculated by the authors and those calculated by Jones⁷ and Matsui¹⁶ are given in Table 6.

(b) Evaluation of $M_+(\alpha/k)$:

$M_+(\alpha/k)$ was formulated in Section 4 and given by (4.17). For convenience, it is rewritten as

$$M_+(\alpha) = M_+(\alpha/k) = e^{\chi(\alpha/k)} M_+^{(1)}(\alpha/k) M_+^{(2)}(\alpha/k), \quad (\text{A.18})$$

in which $\chi(\alpha/k)$ is given by (A.2), and

$$M_+^{(1)}(\alpha/k) = \sqrt{\pi i J_1'(ka)} \prod_{m=1}^{\infty} \left(1 + \frac{\alpha/k}{i\gamma_m'/k}\right) e^{i(\alpha/k)(ka)/m\pi} \quad (\text{A.19})$$

in which

$$\gamma_m'/k = \sqrt{(J_m'/ka)^2 - 1} = -i \sqrt{1 - (J_m'/ka)^2}, \quad (\text{A.20})$$

and J_m' is the ordered zero of $J_1'(x)$.

Also $M_+^{(2)}(\alpha/k)$ in (A.18) is given by

$$M_+^{(2)}(\alpha/k) = \sqrt{H_1^{(1)}(ka)} \left(1 + \frac{\alpha}{k}\right)^{-1} \exp\left[-\frac{ika}{2} + \frac{i\gamma a}{\pi} \ln\left(\frac{\alpha}{k} - \frac{\gamma}{k}\right) + p(\alpha/k)\right], \quad (\text{A.21})$$

in which γ is given by (A.6), and

$$p(\alpha/k) = \frac{1}{\pi} \int_0^{\infty} \left[1 - \frac{2}{\pi x} \left(1 - \frac{1}{x^2}\right) \frac{1}{J_1'^2(x) + Y_1'^2(x)}\right] \cdot \ln\left(1 + \frac{(ka)(\alpha/k)}{\sqrt{(ka)^2 - x^2}}\right) dx. \quad (\text{A.22})$$

In the integrand of (A.22)

$$\sqrt{(ka)^2 - x^2} = i \sqrt{x^2 - (ka)^2}, \text{ for } x > ka.$$

$M_+(\alpha/k)$ has not been calculated before by any author; therefore, the only

TABLE 6

COMPARISON OF SEVERAL VALUES OF $L_+(\alpha/k)$ FOR
 $\alpha/k = 1$ AND DIFFERENT ka

ka	$R_e \{L_+(\alpha/k)\}$			$I_m \{L_+(\alpha/k)\}$		
	L-J-M*	Matsui ¹⁶	Jones ⁷	L-J-M*	Matsui ¹⁶	Jones ⁷
0.1	0.9943	0.9957		0.0614	0.0609	
0.5	0.9059	0.9070	0.9078	0.2726	0.2716	0.2747
1.0	0.7190	0.7205	0.7206	0.4208	0.4196	0.4235
2.0	0.3937	0.3955	0.3942	0.4363	0.4356	0.4391
3.0	0.2351	0.2366	0.2348	0.3137	0.3136	0.3163
5.0	0.2452		0.2439	0.2485		0.2532
7.0	0.1722		0.1705	0.1331		0.1388
10.0	0.1369		0.1305	0.1348		0.1452

*S. W. Lee, V. Jamnejad, Raj Mittra

check on the correctness of the numerical results is a comparison with the low-frequency approximation as given by (6.5) and restated here as

$$M_+(\alpha/k) \approx \frac{i}{ka(1 + \alpha/k)} \left\{ 1 + \frac{(ka)^2}{4} [1 - (\alpha/k)^2] \ln[ka(1 + \alpha/k)] \right\} \quad (\text{A.23})$$

for $k^2 a^2, |\alpha|^2 a^2 \ll 1$.

$L_+(\alpha/k)$ and $M_+(\alpha/k)$, as can be seen from (A.1) and (A.18), are very similar and one may expect similar methods for their numerical computation; this is indeed the case. The product factor in (A.19) is identical to that of (A.3) as given explicitly by (A.9), upon replacing γ_m by γ'_m . This product is convergent and, as before, is calculated by using a suitable choice of the upper limit M . The first few values of J'_m are found in the tables,¹⁵ and for large values of m , the asymptotic formula

$$J'_m = \beta' - \frac{7}{8\beta'}; \quad \beta' = (m - \frac{1}{4})\pi \text{ as } m \rightarrow \infty \quad (\text{A.24})$$

is used. The behavior of the product when the value of M is increased is very similar to the previous case for $L_+(\alpha/k)$, and consequently the value of $M = 300$ is chosen.

Evaluation of the Cauchy principal value of the integral in (A.22) follows along a line similar to the previous case of (A.7). In short, the behavior of the integral is investigated through the evaluation of an integral of the form given by (A.11) thus producing an approximate formula similar to (A.12). Consequently, it may be shown that the integral is well-behaved around the point $x = ka$ and can be evaluated by a formula similar to (A.13). The investigation of the behavior of the integrand in (A.22) for large values of x can be similarly approached. The first part of the integrand has an asymptotic behavior of the form

$$\left[1 - \frac{2}{\pi x} \left(1 - \frac{1}{x^2} \right) \cdot \frac{1}{J_1'(x) + Y_1'^2(x)} \right] \xrightarrow{x \rightarrow \infty} \frac{7}{8} \frac{1}{x^2}. \quad (\text{A.25})$$

The second part of the integrand in (A.22) is identical to that of (A.7) as given by (A.15). Again it can be concluded that the absolute value of the integrand in (A.22), for large values of x , is of the order $(1/x^3)$. Therefore, by choosing an upper limit $x = x_{\max}$ for the integral in (A.22), the disregarded part of the integral will be of the order $(1/x_{\max}^2)$.

The integrand of (A.22) assumes the following approximate value as x approaches zero,

$$\frac{1}{\pi} \left[1 - \frac{2}{\pi x} \left(1 - \frac{1}{x^2} \right) \cdot \frac{1}{J_1'(x) + Y_1'^2(x)} \right] \ln \left(1 + \frac{(ka)(\alpha/k)}{\sqrt{(ka)^2 - x^2}} \right) \xrightarrow{x \rightarrow \infty} \frac{1}{\pi} \left(1 + \frac{\pi}{2} x \right) \ln[1 + (\alpha/k)]. \quad (\text{A.26})$$

Considering the preceding discussion, the obtained results in (A.11), (A.12), (A.25), (A.26), and some actual numerical evaluations, the behavior of the integrand in (A.22) can be summarily given as follows. The absolute value of the integrand starts from a certain value at $x = 0$. Then, in the case $x \lesssim 0.5$, the absolute value slightly increases until it reaches the neighborhood of $x = ka$, whereupon it rapidly goes to infinity at $x = ka$. However, if $x \gtrsim 0.5$, the absolute value of the integrand finds a low maximum around $x \approx 0.5$, then decreases and finds a minimum in the neighborhood of $x = ka$; whereupon it rapidly ascends to infinity. (Note that the occurrence of the low maximum at $x \approx 0.5$ is peculiar to (A.22) for $M_+(\alpha/k)$ and does not occur in the corresponding case of $L_+(\alpha/k)$. Then, after the point $x = ka$, the absolute value of the integrand drops rapidly from infinity and eventually goes

to zero as x goes to infinity. A typical behavior of the integrand of $p(\alpha/k)$, as given in (A.22), is presented in Figure 12. It is apparent that the integrand of $P(\alpha/k)$ converges to zero slower than that of $q(\alpha/k)$. Therefore, in the former case the upper limit of the integration will be considered larger than the latter case and is given by

$$x_{\max} = \text{constant} + ka = 5 + ka. \quad (\text{A.27})$$

Following the considerations of the case of $q(\alpha/k)$ in (A.7), the integral will be evaluated numerically using the Gaussian quadrature method of integration and considering two intervals, i.e., $(0 \rightarrow ka)$ and $(ka \rightarrow x_{\max})$. In Table 7, some calculated values of $M_+(\alpha/k)$ are given. As a check on the correctness of the results, a comparison with the low-frequency approximations obtained from (A.23) is also given in Table 7.

As a final comment on the calculation of $L_+(\alpha/k)$ and $M_+(\alpha/k)$, it may be observed that factorization formulas for the Wiener-Hopf kernels as given by (4.3) and (4.4) can be used to check both the accuracy of the factorization process and the numerical computation by calculating the right- and left-hand side of the aforementioned formulas separately and comparing the results. Now the field and related quantities may be computed.

(c) Evaluation of the scattered field and distortion parameter:

Formulation of the scattered magnetic field due to the axial incidence of a field of the form $e^{-i(kz)}$ (time dependence $e^{-i\omega t}$ is implicitly assumed) on a semi-infinite hollow cylinder, has been given in Section 5. For convenience, it is rewritten in a form suitable for numerical evaluation.

$$H_x(\rho, \phi, z) = \frac{ka}{N_+(1)} (h_1 + h_2), \quad 0 < kz < \infty \quad (\text{A.28})$$

in which $N_+(\alpha/k)$ is given by

TABLE 7

COMPUTED VALUES OF $M_+(\alpha/k)$ IN THE GENERAL CASE AND IN THE LOW-FREQUENCY APPROXIMATION

α/k	ka	$M_+(\alpha/k)$	
		General Case	Low-Frequency Approximation
1.	0.1	0.294+i4.997	15
	0.2	0.295+i2.505	12.5
	0.3	0.294+i1.677	11.67
	0.5	0.290+i1.021	11.
	1.	0.264+i0.525	10.5
	3.	0.340+i0.315	—
	5.	0.179+i0.201	—
	7.	0.184+i0.211	—
	10.	0.157+i0.172	—

$$N_+(\alpha/k) = 4(ka)^2 M_+^2(\alpha/k) - L_+^2(\alpha/k). \quad (\text{A.29})$$

In Equation (A.28), h_1 is given by

$$h_1 = - \int_0^1 \left\{ L_+(1) \frac{J_1(\kappa \cdot ka)}{\kappa L_+(\alpha/k)} f_1(\rho, \phi) + 2ka M_+(1) \frac{(\alpha/k)}{1 + (\alpha/k)} \frac{J_1'(\kappa \cdot ka)}{M_+(\alpha/k)} \cdot f_2(\rho, \phi) \right\} \cdot e^{i(\alpha/k)(kz)} d\left(\frac{\alpha}{k}\right) \quad (\text{A.30})$$

in which

$$\kappa = + \sqrt{1 - (\alpha/k)^2}$$

$$f_1(\rho, \phi) = \begin{cases} 1, & \text{if } \rho = 0 \\ 2 \left[\frac{J_1(\kappa \cdot k\rho)}{\kappa \cdot k\rho} - J_2(\kappa k\rho) \cos^2 \phi \right], & \text{otherwise,} \end{cases} \quad (\text{A.31})$$

and

$$f_2(\rho, \phi) = \begin{cases} 1, & \text{if } \rho = 0 \\ 2 \left[\frac{J_1(\kappa \cdot k\rho)}{\kappa \cdot k\rho} - J_2(\kappa k\rho) \sin^2 \phi \right], & \text{otherwise.} \end{cases} \quad (\text{A.32})$$

Also h_2 in (A.28) is given by

$$h_2 = \int_0^\infty \left\{ 2(ka) M_+(1) \frac{-(\beta/k)}{1 + i(\beta/k)} \frac{J_1'(\bar{\kappa}ka)}{M_+(i\beta/k)} f_1(\rho, \phi) + iL_+(1) \frac{J_1(\bar{\kappa}ka)}{\bar{\kappa} \cdot L_+(i\beta/k)} f_2(\rho, \phi) \right\} e^{-(\beta/k)(kz)} d\left(\frac{\beta}{k}\right) \quad (\text{A.33})$$

in which

$$\bar{\kappa} = + \sqrt{1 + (\beta/k)^2},$$

and functions f_1 and f_2 are given by (A.31) and (A.32) upon substituting

$\bar{\kappa}$ for κ . Then the total magnetic field will be given by the equation

$$H_x^{(t)}(\rho, \phi, z) = H_x(\rho, \phi, z) + e^{-i(kz)}. \quad (\text{A.34})$$

In addition, the distortion parameter as defined in (5.19) will be given by

$$D(\rho, \phi, z) = e^{i(kz)} \cdot H_x(\rho, \phi, z). \quad (\text{A.35})$$

The main step in the numerical evaluation of the field quantities is the computation of h_1 and h_2 , as given in (A.30) and (A.33). h_1 can be easily evaluated by using the 16-point Gaussian method of integration in the interval [0-1]. However, the evaluation of h_2 in (A.33) merits special attention. As may be noted, the integral extends to infinity, but due to the exponentially decaying term in the integrand, we may disregard the integrand for values of (β/k) larger than a suitable limit $(\beta/k) = x_{\max}$. This limit should be inversely proportional to (kz) . Bearing this limitation in mind, several sub-intervals of integration are considered within the interval $[0, x_{\max}]$. The sub-intervals have been chosen as follows:

$$\begin{aligned} [0., 1.], [1., 3.], [3., 7.], [7., 12.] & \quad \text{for } kz \leq 0.8, \\ [0., 0.6], [0.6, 1.5], [1.5, 4.] & \quad \text{for } 0.8 < kz \leq 2., \\ [0., 0.2], [0.2, 0.8], [0.8, 2.] & \quad \text{for } 2. < kz < 10. \end{aligned}$$

With these provisions, different field quantities are computed and the results obtained are given in Section 7.

A low-frequency approximation to the field quantities, as explained in Section 6, may be obtained by considering the formulas,

$$\int h_1 \approx \frac{1}{2} \frac{ka}{kz} \left(2 - \frac{1}{ikz}\right) e^{ikz} - \frac{1}{2} \frac{ka}{kz} \left(1 - \frac{1}{ikz}\right), \quad (\text{A.36})$$

$$h_2 \approx \frac{1}{2} \frac{ka}{kz} \left(1 - \frac{1}{ikz}\right); \quad \rho = 0, \quad ka \ll 1, \quad kz > ka. \quad (\text{A.37})$$

These approximate formulas lead to the following result for the scattered magnetic field,

$$H_x(\rho = 0, z) \approx \frac{-ka}{2} \frac{ia}{2z} \left(2 - \frac{1}{ikz}\right) e^{ikz} \quad (\text{A.38})$$

$$\rho = 0, ka \ll 1, z > a.$$

Finally, the approximate values of the total field and the distortion parameter can be immediately evaluated substituting (A.38) in (A.34) and (A.35). A comparison of the results obtained for the scattered field by the general formulas and by the low-frequency approximation is done in Section 7 and demonstrated in Figure 10.

(d) Evaluation of the currents:

Formulation of the current on the surface of a semi-infinitely hollow cylinder due to the presence of an axial incident field of the spatial form $e^{-i(kz)}$ is done in Section 5. The final results are repeated in a form convenient for the numerical evaluation.

$$\frac{J_z}{\sin \phi} = \frac{4}{\pi^2 N_+(1)} (I_1 + I_2), \quad -\infty < kz < 0 \quad (\text{A.39})$$

$$\frac{J_\phi}{\cos \phi} = \frac{-8i}{\pi^2} \frac{(ka)M_+(1)}{N_+(1)} (I_3 + I_4), \quad -\infty < kz < 0 \quad (\text{A.40})$$

in which $N_+(\alpha/k)$ is given by (A.29). Components $I_1, I_2, I_3,$ and I_4 in (A.39) and (A.40) are given by

$$I_1 = \int_0^1 \left\{ \frac{2(\alpha/k)}{1 - (\alpha/k)} \frac{M_+(1)M_+(\alpha/k)}{J_1'^2(\kappa ka) + Y_1'^2(\kappa ka)} + \frac{L_+(1)L_+(\alpha/k)}{J_1^2(\kappa ka) + Y_1^2(\kappa ka)} \right\} \cdot \frac{e^{-i(\alpha/k)(kz)}}{1 - (\alpha/k)^2} d\left(\frac{\alpha}{k}\right), \quad (\text{A.41})$$

$$I_2 = -i \int_0^{\infty} \left\{ \frac{2i(\beta/k)}{1 - i(\beta/k)} \frac{M_+(1)M_+(i\beta/k)}{J_1'^2(\bar{\kappa}ka) + Y_1'^2(\bar{\kappa}ka)} + \frac{L_+(1)L_+(i\beta/k)}{J_1^2(\bar{\kappa}ka) + Y_1^2(\bar{\kappa}ka)} \right\} e^{+(\beta/k)(kz)} \frac{e}{1 + (\beta/k)^2} d\left(\frac{\beta}{k}\right), \quad (A.42)$$

$$I_3 = \int_0^1 \frac{M_+(\alpha/k)}{(1 - \alpha/k)[J_1'^2(\kappa ka) + Y_1'^2(\kappa ka)]} e^{-i(\alpha/k)(kz)} d\left(\frac{\alpha}{k}\right), \quad (A.43)$$

and

$$I_4 = -i \int_0^{\infty} \frac{M_+(i\beta/k)}{(1 - i\beta/k)[J_1'^2(\bar{\kappa}ka) + Y_1'^2(\bar{\kappa}ka)]} e^{+(\beta/k)(kz)} d\left(\frac{\beta}{k}\right). \quad (A.44)$$

In the formulas (A.41), (A.42), (A.43), and (A.44), κ and $\bar{\kappa}$ are given by

$$\kappa = \sqrt{1 - (\alpha/k)^2}, \quad \bar{\kappa} = \sqrt{1 + (\beta/k)^2}. \quad (A.45)$$

Evaluation of I_1 and I_3 is readily obtained by using the 16-point Gaussian method of integration in the integral $[0, 1]$. However, special attention should be given to the infinite limit of integrals for I_2 and I_4 as given by (A.42) and (A.44). Since we are concerned with the case of $z < 0$, it is apparent that the exponential terms in the integrands of (A.42) and (A.44) have a decaying behavior. Therefore, a maximum limit for the interval of integration in (A.42) and (A.44) may be chosen (albeit inversely proportional to kz), such that the remainder of the integrals can be disregarded. Within this limit the interval of integration has been divided into several sub-intervals and the 16-point Gaussian method of integration has been employed in every sub-interval. The sub-intervals are

given by

[0., 1.], [1., 3.], [3., 7.], [7., 12.], for $kz \geq -0.8$

[0., 0.6], [0.6, 1.5], [1.5, 4.], for $-0.8 > kz \geq -2.$

and

[0., 0.2], [0.2, 0.8], [0.8, 2.], for $-0.2 > kz > -10.$

With these provisions, the circumferential and longitudinal currents have been computed from (A.37) and (A.40), and the obtained results are given in Section 7.

In this case also, a low-frequency approximation to the currents, as explained in Section 6, may be obtained by the following formulas,

$$\frac{J_z}{\sin \phi} \approx \frac{1}{2} \left(\frac{ka}{kz}\right)^2 e^{-ikz}, \quad ka \ll 1, \quad |kz| \gg ka \quad (\text{A.46})$$

and

$$\frac{J_\phi}{\cos \phi} \approx \left(\frac{ka}{kz}\right)^3 (1 + ikz) e^{-ikz}, \quad ka \ll 1, \quad |kz| \gg ka. \quad (\text{A.47}).$$

A comparison of the general and approximate results for the circumferential current was given in Section 7 and was demonstrated in Figure 11. Unfortunately, the results obtained for the longitudinal current by the general formulas in the low-frequency range are not reliable. This occurs because the errors in the numerical evaluation of I_1 and I_2 are cumulative; and since the current has a very small value which is comparable to the total error, the error plays a decisive role in the determination of the final result. The longitudinal currents as computed from (A.39) and from (A.46) are compared in Figure 13. Since the amount of error in the numerical evaluation of (A.39) could not

be decreased for low frequencies, therefore, in such cases, the use of the approximate formula as given by (A.46) should be preferred.

LIST OF REFERENCES

1. C. E. Baum, "Some electromagnetic considerations for a rocket platform for electromagnetic sensors," *Sensor and Simulation Note* 56, June 1968.
2. R. W. Latham and K. S. H. Lee, "Magnetic-field distortion by a specific axisymmetric, semi-infinite, perfectly conducting body," *Sensor and Simulation Note* 102, April 1970.
3. C. E. Baum, "Two approaches to the measurement of pulsed electromagnetic fields incident on the surface of the earth," *Sensor and Simulation Note* 109, June 1970.
4. H. Levine and J. Schwinger, "On the radiation of sound from an unflanged circular pipe," *Phys. Rev.*, 73, pp. 383-406, 1948.
5. J. E. Pearson, "Diffraction of electromagnetic waves by a semi-infinite circular wave guide," *Proc. Camb. Philos. Soc.*, 49, pp. 659-667, 1953.
6. L. A. Vajnshtein, "Propagation in semi-infinite wave guides," NYU Res. Rept. EM-63, Institute of Math. Sci., New York University, New York, 1954.
7. D. S. Jones, "The scattering of a scalar wave by a semi-infinite rod of circular cross section," *Philos. Trans. Roy. Soc. London, Ser. A*, 247, pp. 499-528, 1955.
8. J. J. Bowman, "Scattering of plane electromagnetic waves from a semi-infinite hollow circular pipe," Memo D0620-125-M41-10, and Memo D0620-127-M41-13, Conduction Corp., Ann Arbor, Michigan, 1963.
9. O. Einarsson, R. E. Kleinman, P. Laurin, and P. L. E. Uslenghi, "Studies in radar cross sections L-diffraction and scattering by regular bodies IV: the circular cylinder," Rept. 7133-3-T, Radiation Lab, University of Michigan, Ann Arbor, Michigan.
10. C. C. Kao, "Electromagnetic scattering from a finite tubular cylinder: numerical solution," *Radio Science*, 5, no. 3, March 1970.
11. P. M. Morse and H. Feshbach, *Methods of Theoretical Physics*, McGraw-Hill Book Co., 1953.
12. B. Noble, *Methods Based on Wiener-Hopf Technique*, Pergamon Press, New York, 1958.
13. D. S. Jones, *The Theory of Electromagnetism*, Macmillan Co., New York, 1964.
14. R. Mittra and S. W. Lee, *Analytical Techniques in the Theory of Guided Waves*, Macmillan Co., New York, 1971.

15. M. Abramowitz, I. A. Stegun, Handbook of mathematical functions, Dover Publications, Inc., New York, 1965.
16. E. Matsui, "On the free-field correction for laboratory standard microphones mounted on a semi-infinite rod," NBS Rept. No. 7038, 1960.

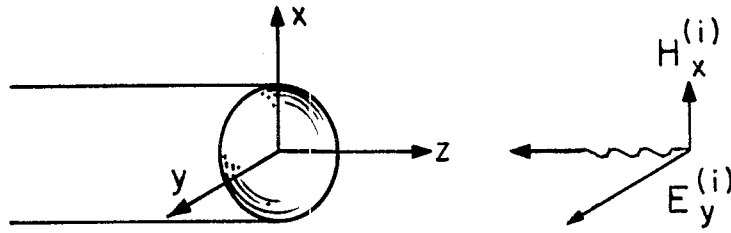


Figure 1. Scattering of a plane wave by a semi-infinite, hollow, conducting cylinder

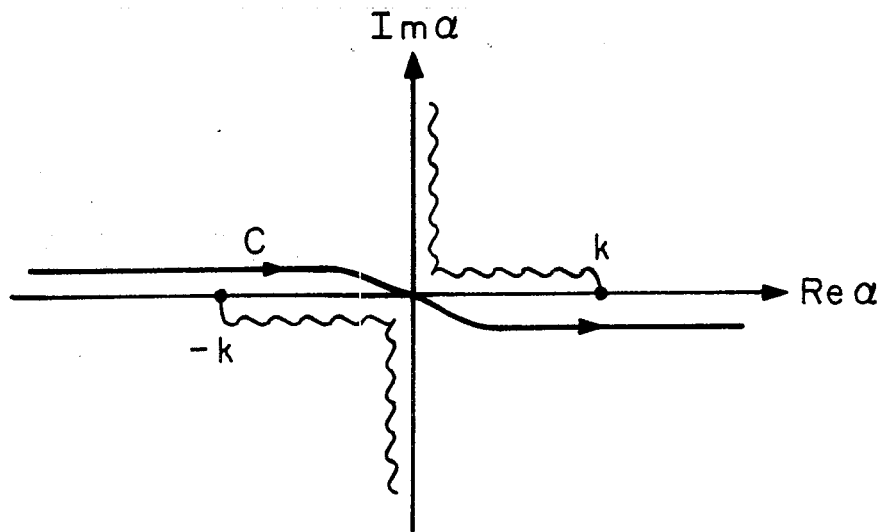


Figure 2. Branch cuts for $\kappa = \sqrt{k^2 - \alpha^2}$ in the α -plane

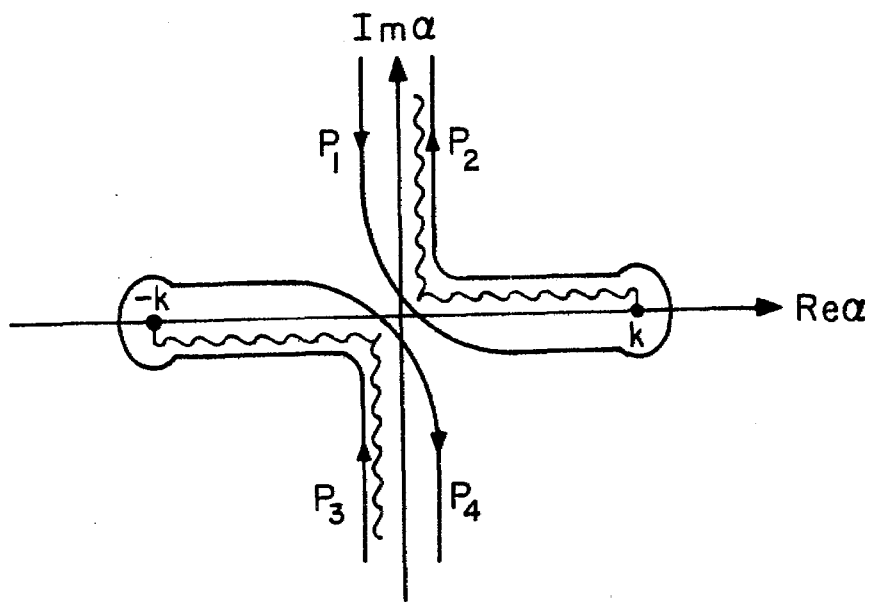


Figure 3. Contour P in the complex α -plane

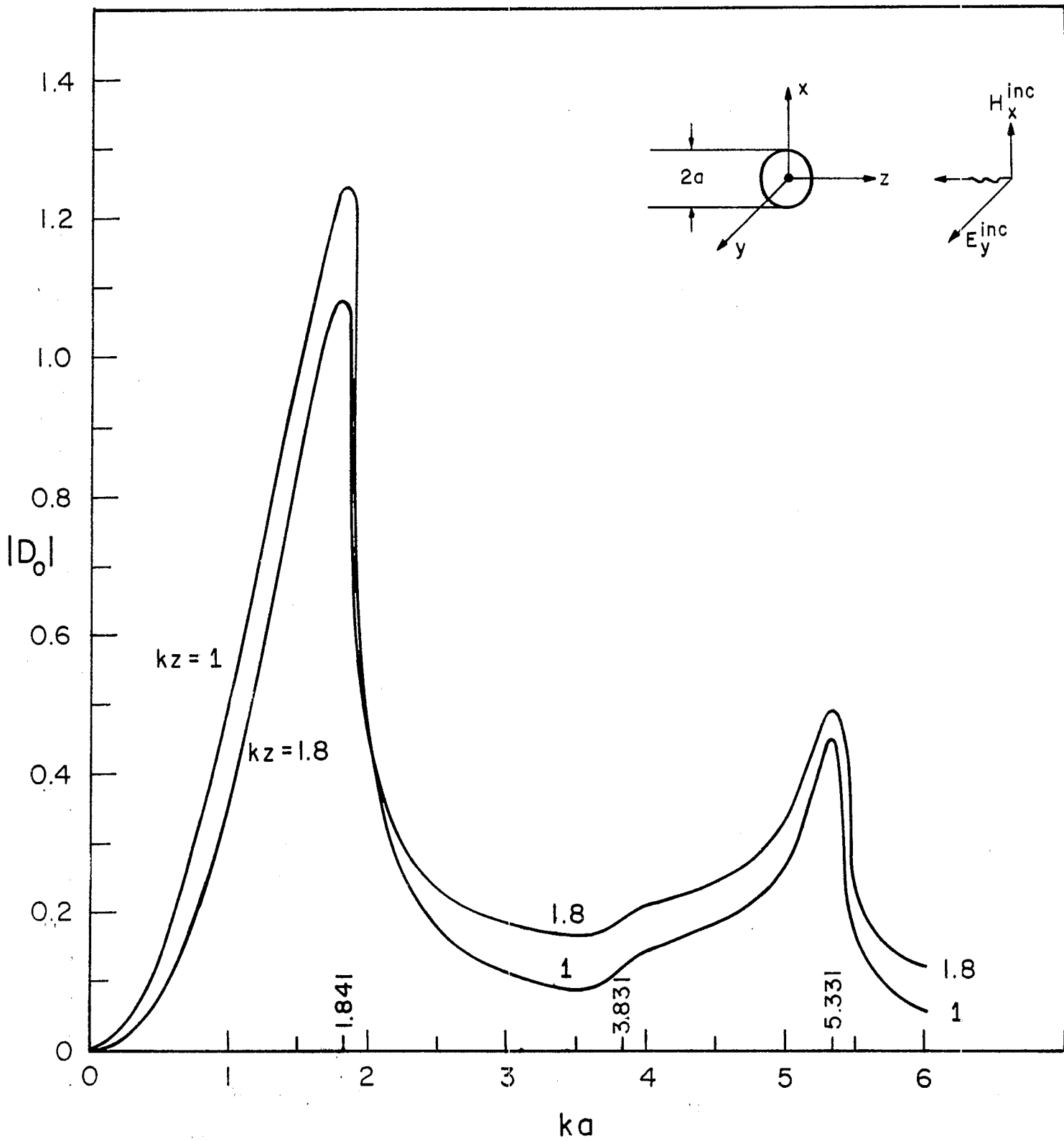


Figure 4. Absolute value of distortion parameter D_0 defined in Equation (7.1) (or the scattered H_x) versus ka for a given kz

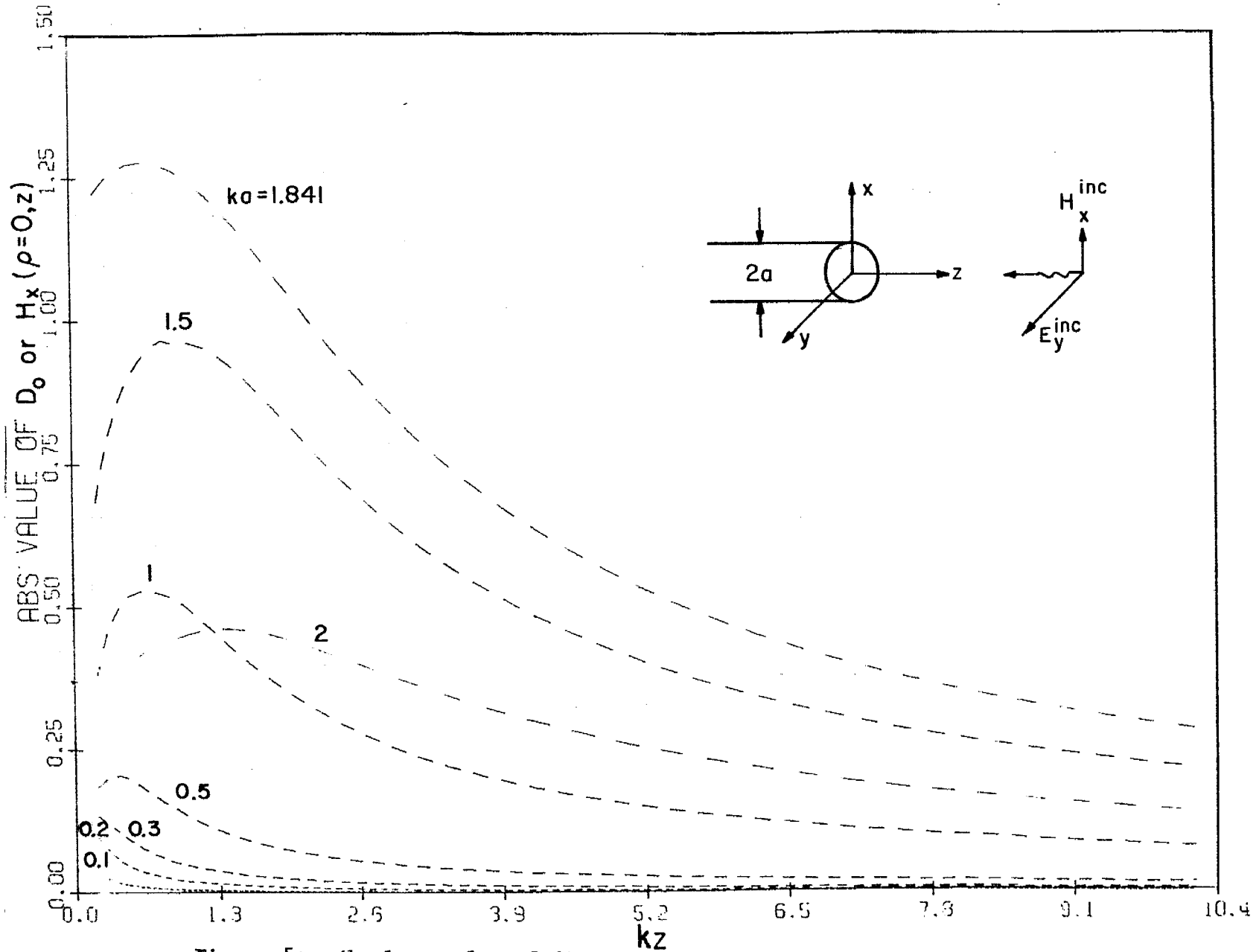


Figure 5a. Absolute value of distortion parameter D_0 as defined in Equation (7.1) or that of the scattered field H_x^0 versus kz for a given ka

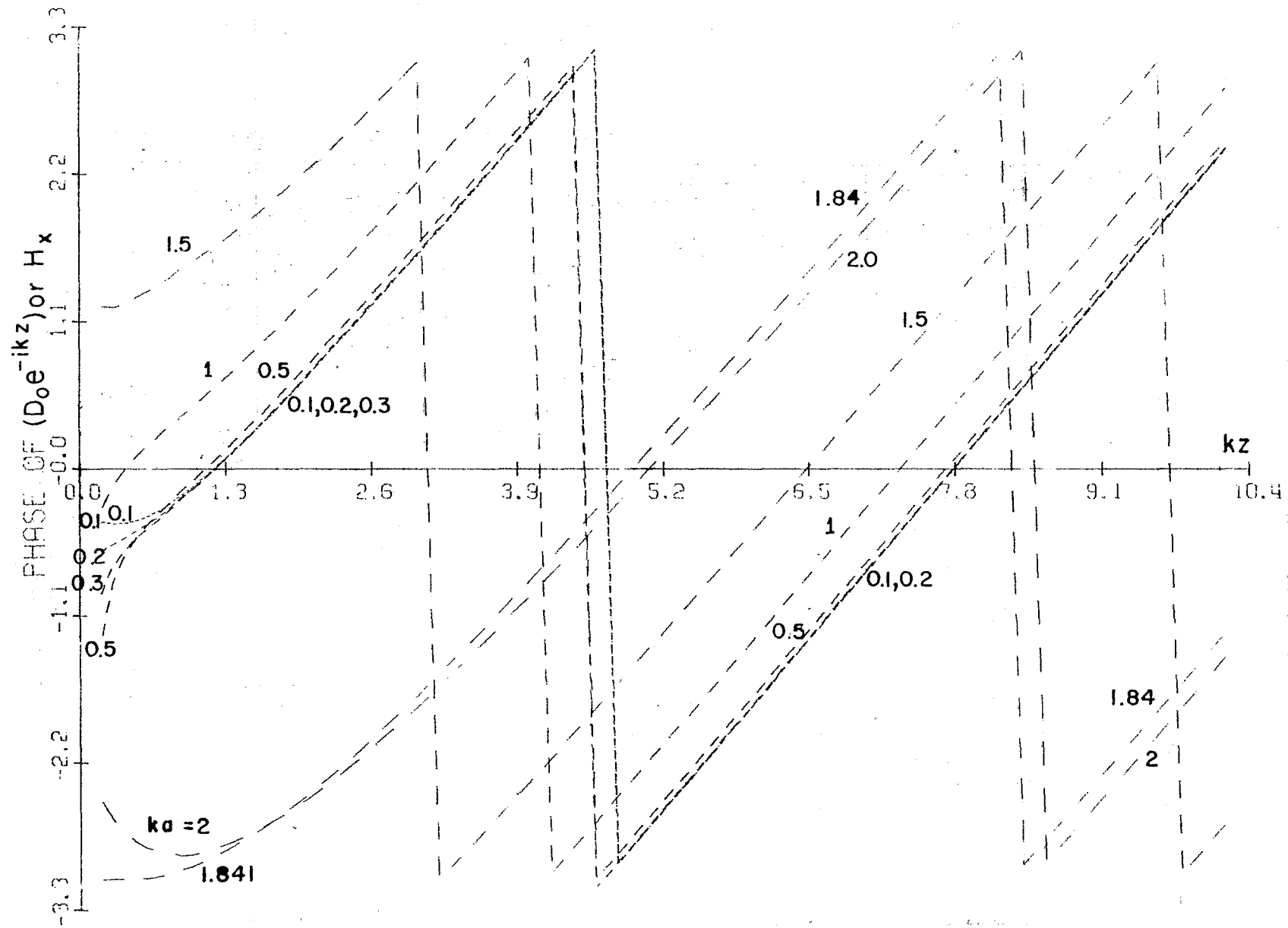


Figure 5b. Phase of distortion parameter D as defined in Equation (7.1), (or that of the scattered field H_x^0) versus kz for a given ka

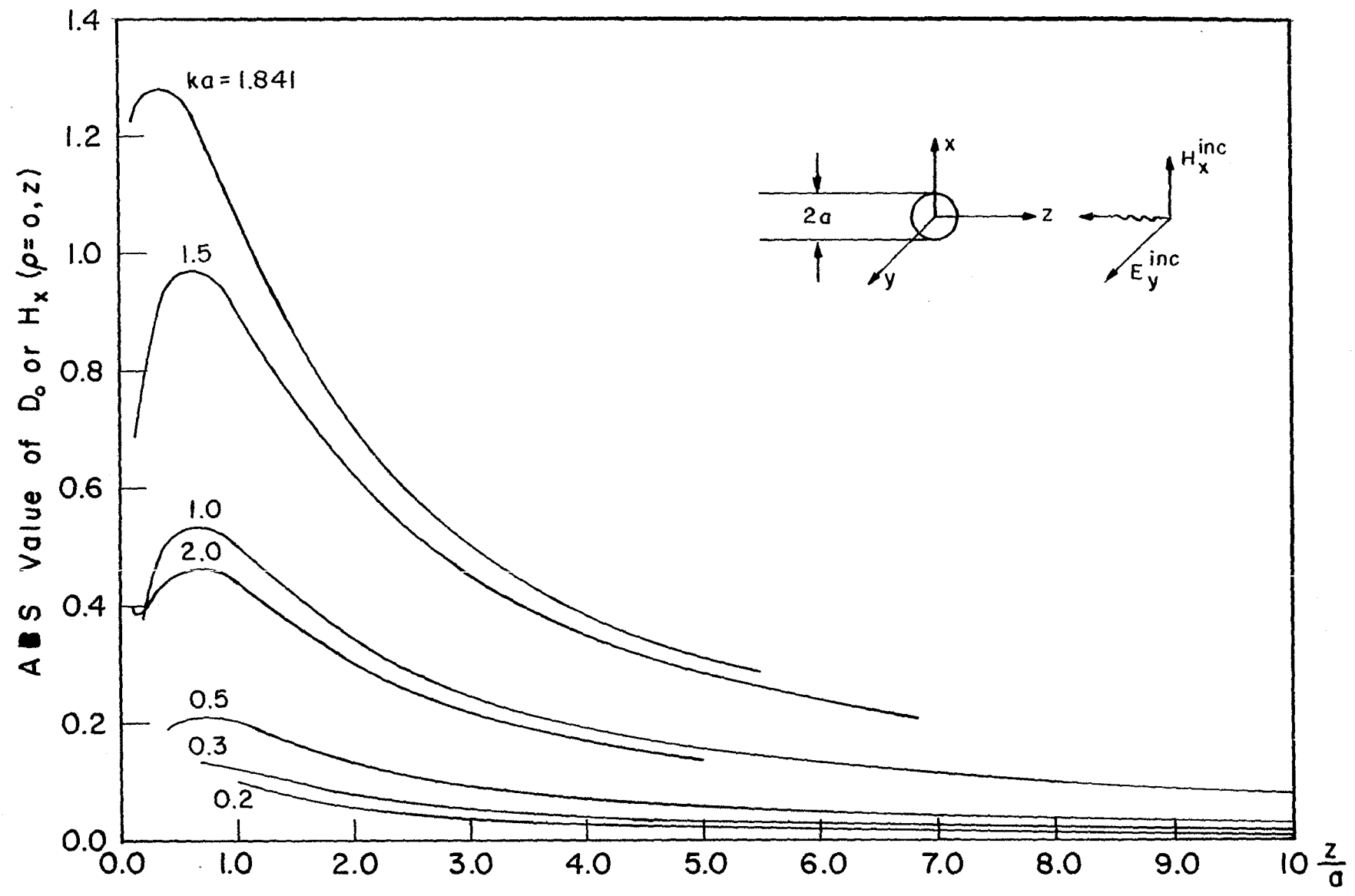


Figure 6. Absolute value of distortion parameter D_0 as defined in Equation (7.1) versus z/a for given ka

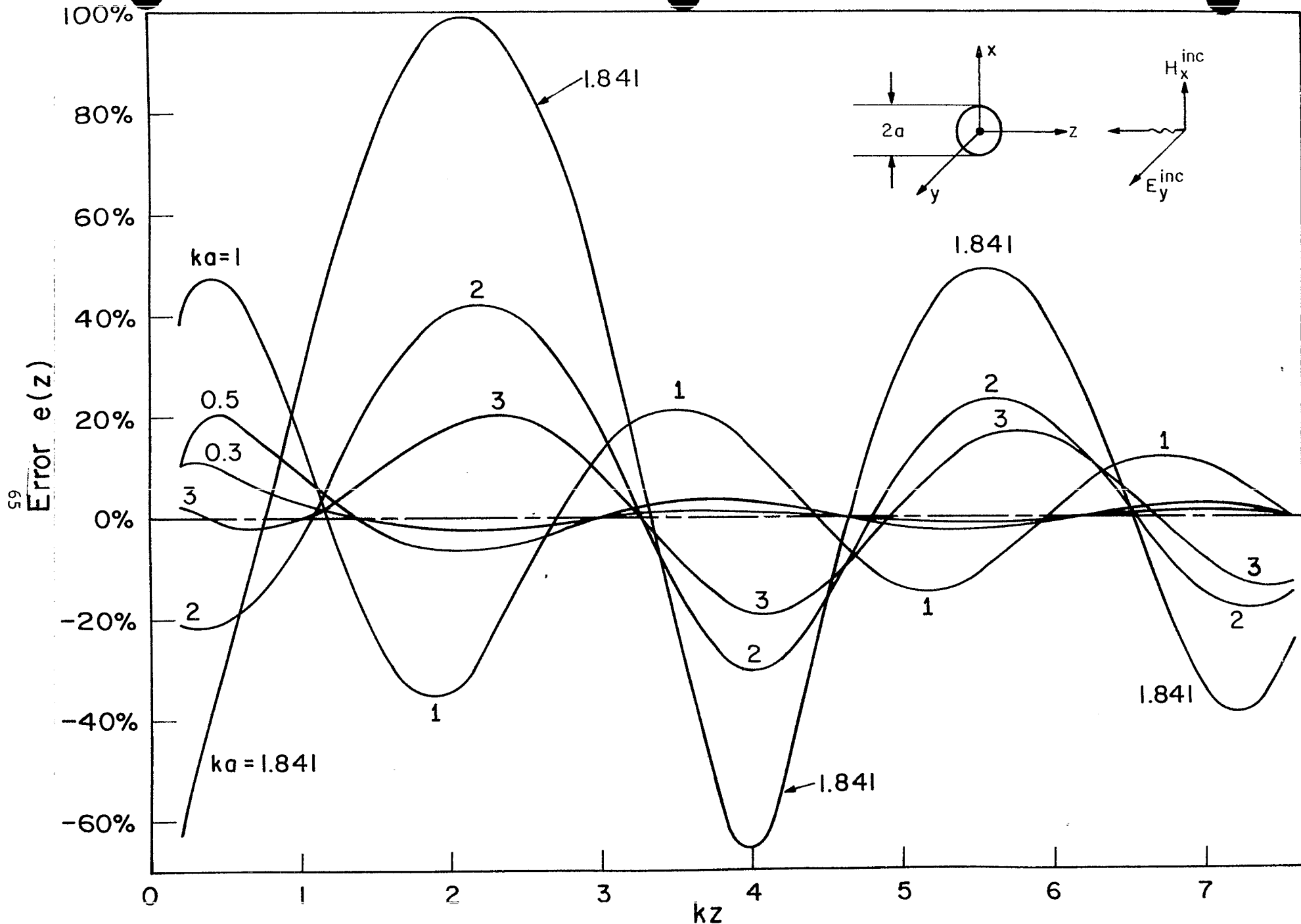


Figure 7. Error in the measurement of EMP due to the sensor boom at a given frequency as defined in Equation (7.5)

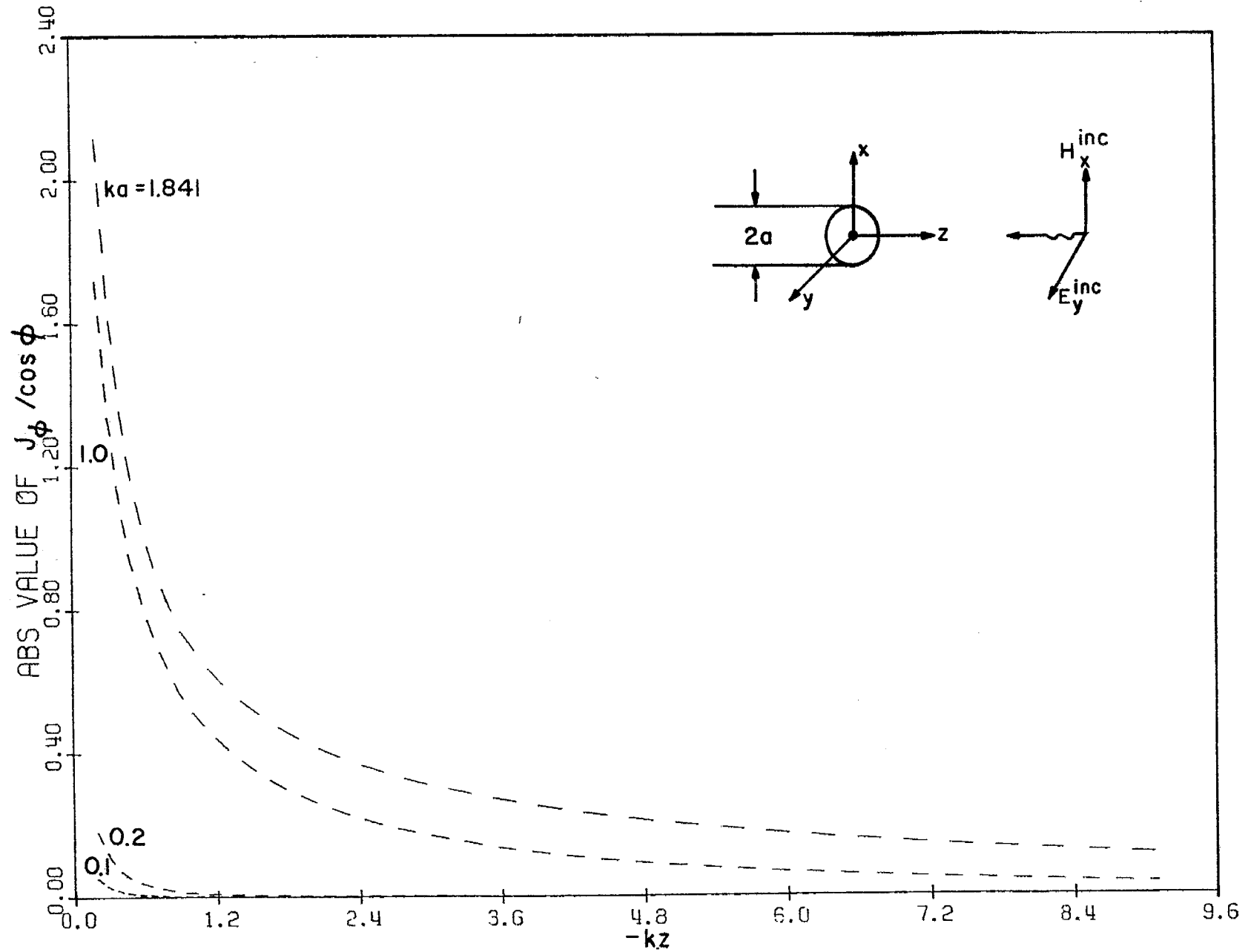


Figure 8a. Absolute value of the circumferential current J_ϕ versus kz for a given ka

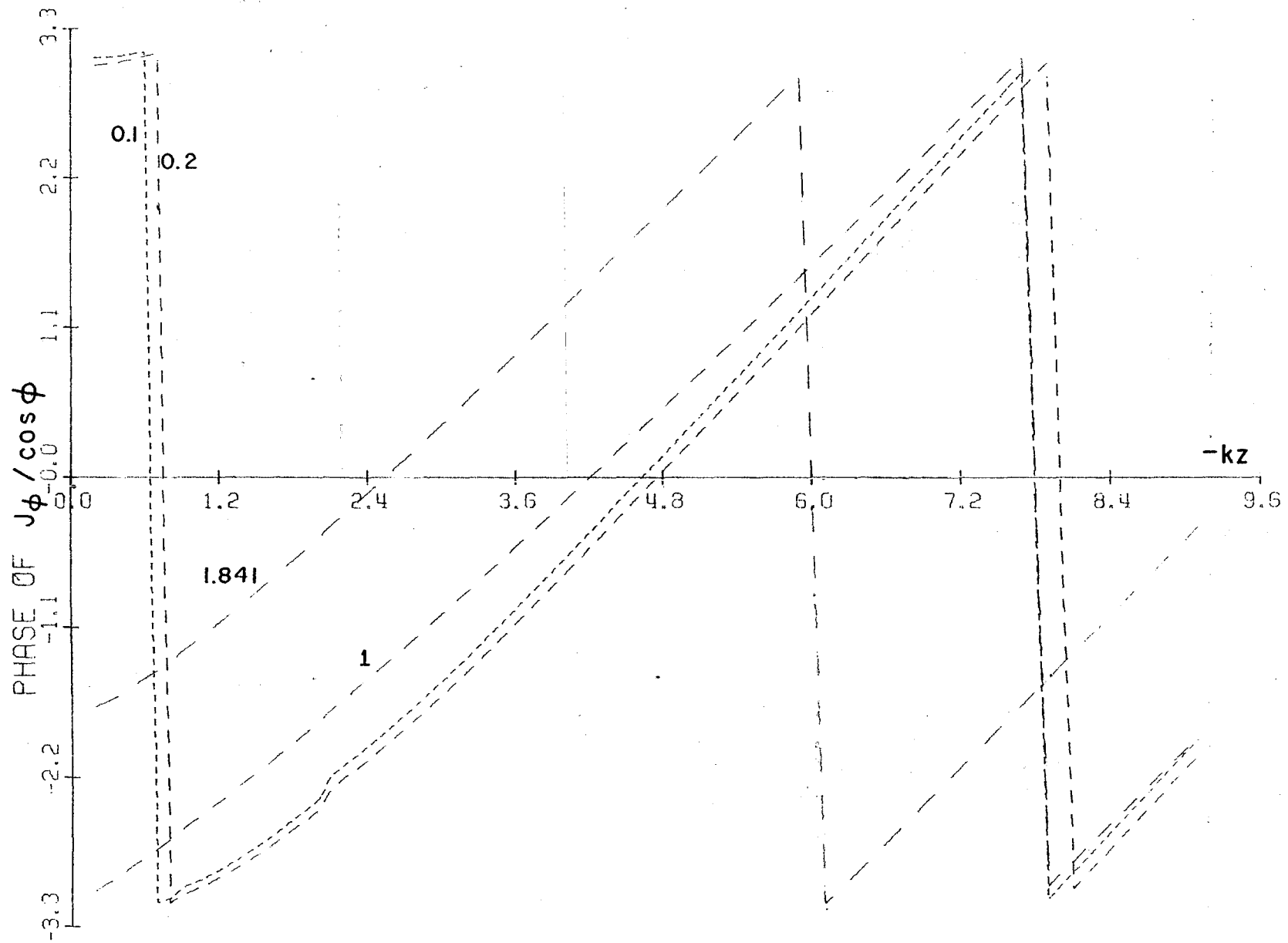


Figure 8b. Phase of the circumferential current J_ϕ versus kz for a given ka

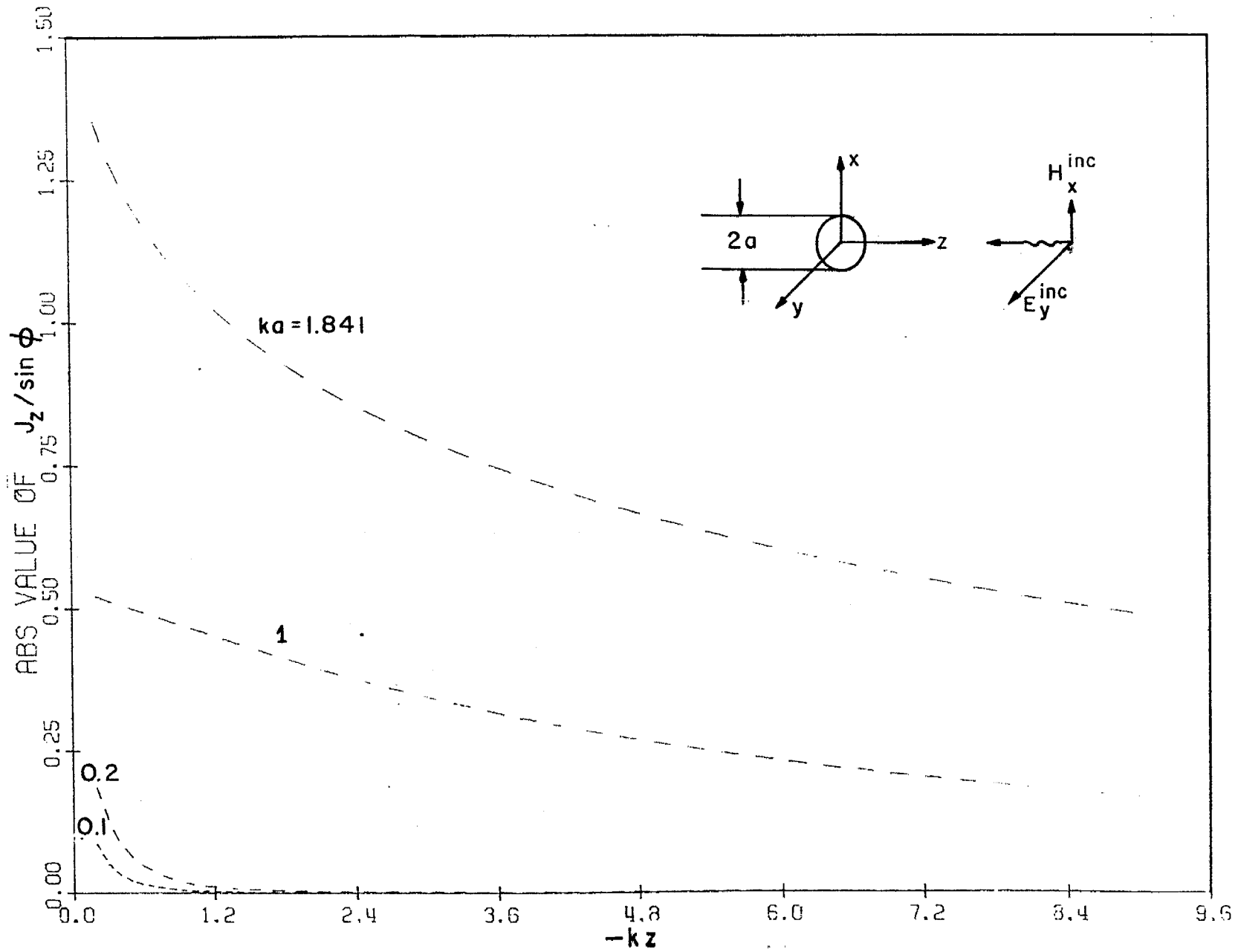


Figure 9a. Absolute value of the axial current J_z versus kz for a given ka

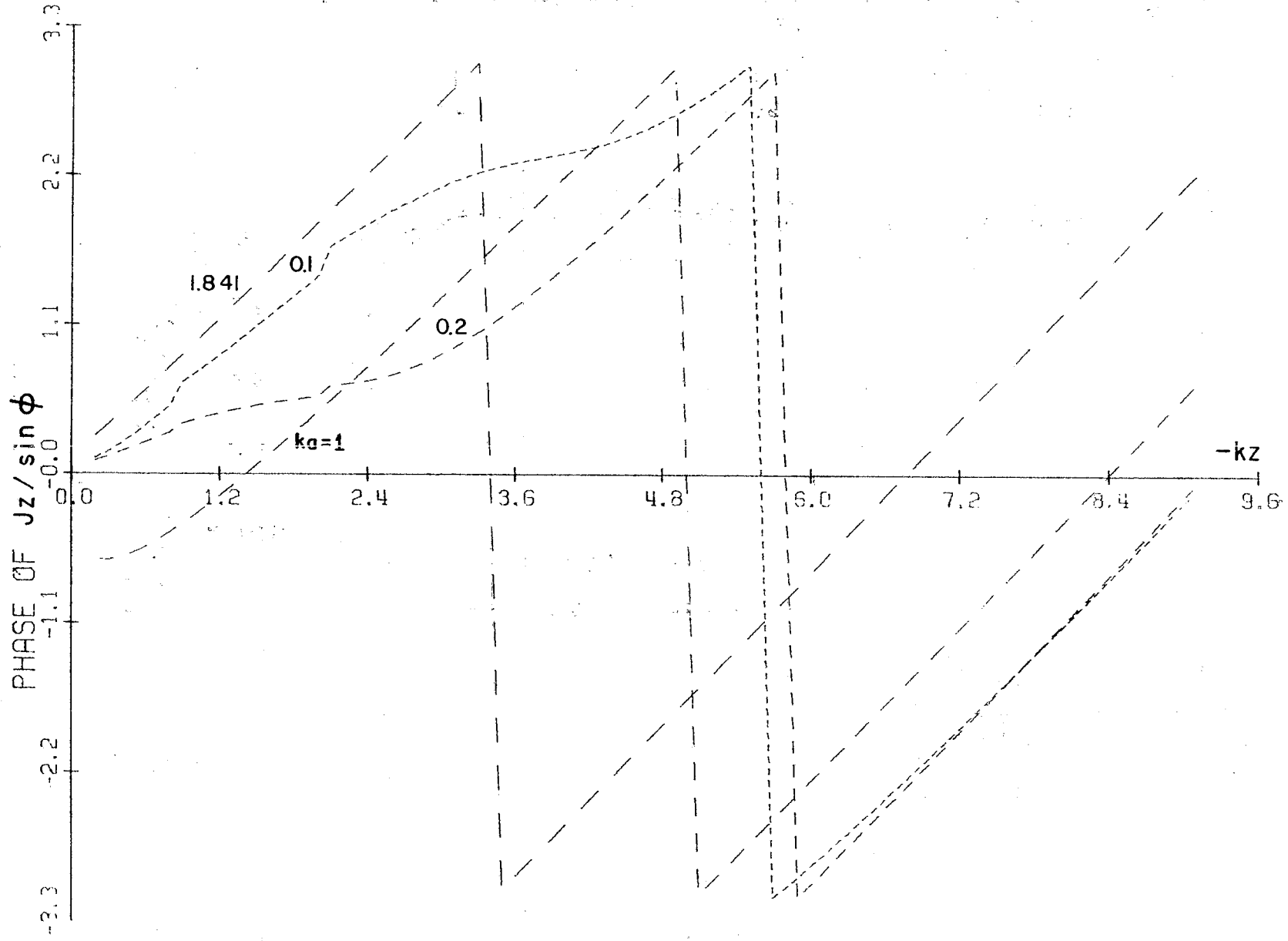


Figure 9b. Phase of the axial current J_z versus kz for a given ka

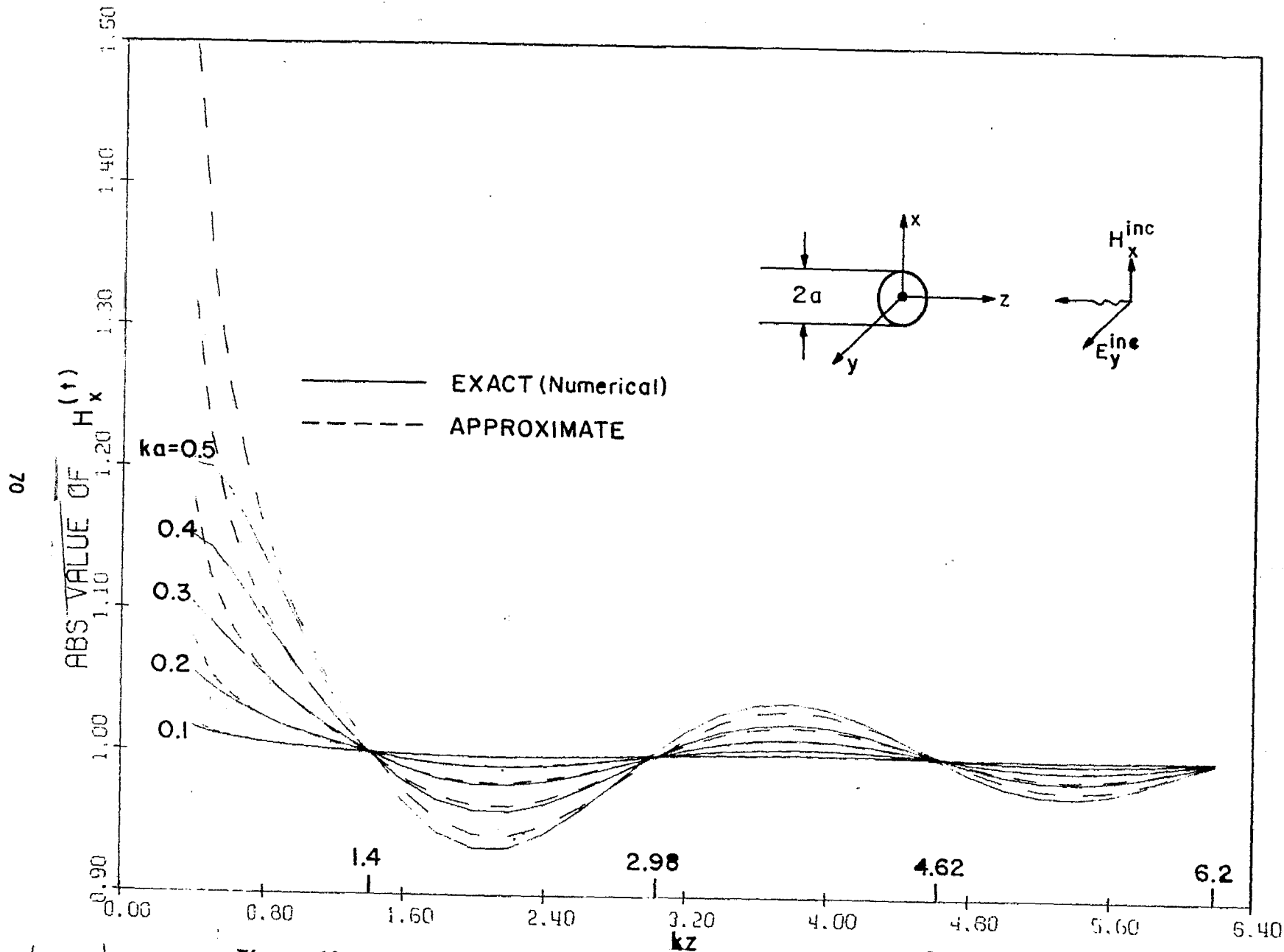


Figure 10a. Comparison of the absolute value of the total field $H_x(t)$ as computed from general formulas in Section 5 and from the low-frequency approximations in Section 6

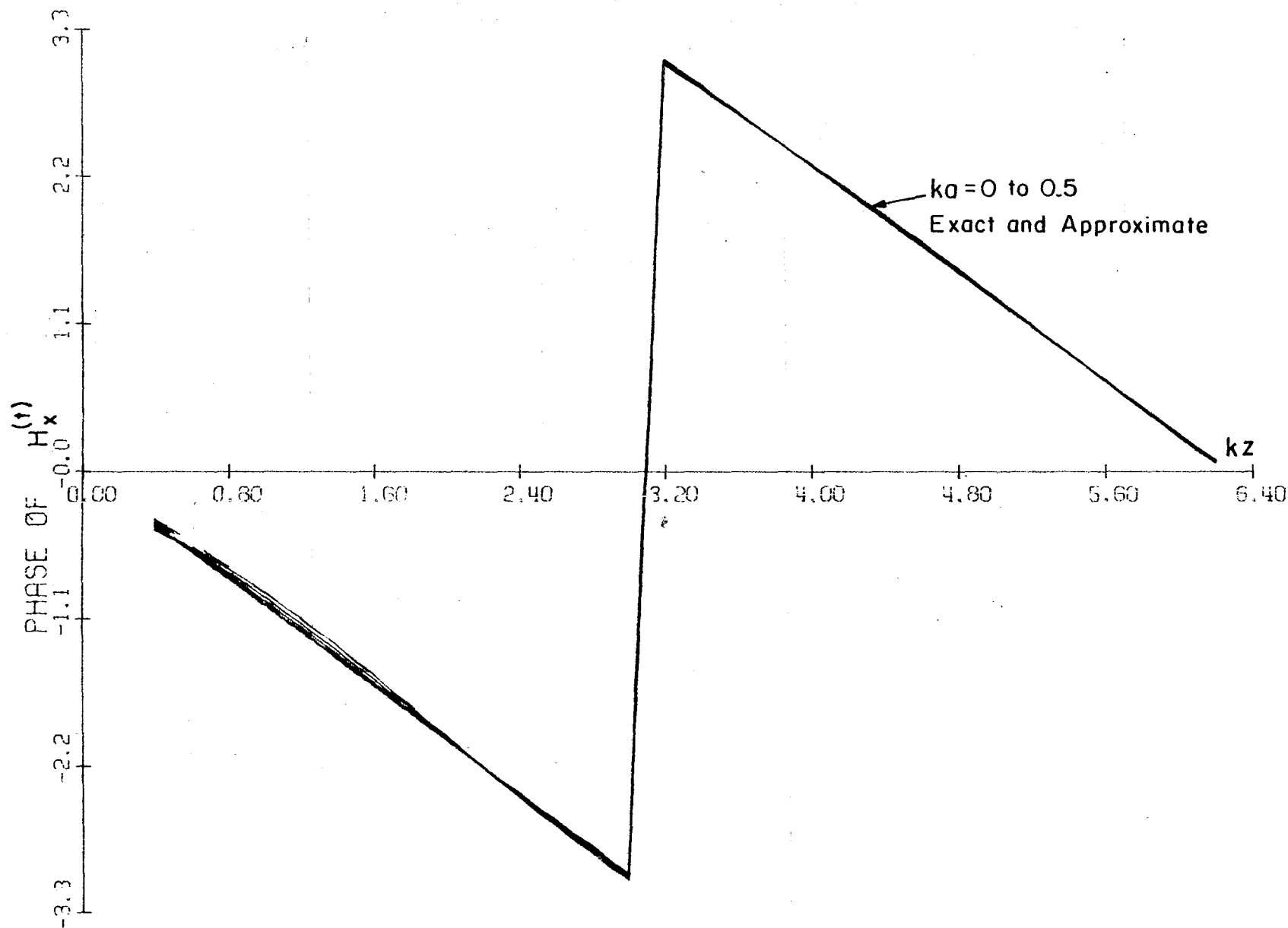


Figure 10b. Comparison of the phase of the total field $H_x^{(t)}$ as computed from general formulas in Section 5 and from low-frequency approximations in Section 6

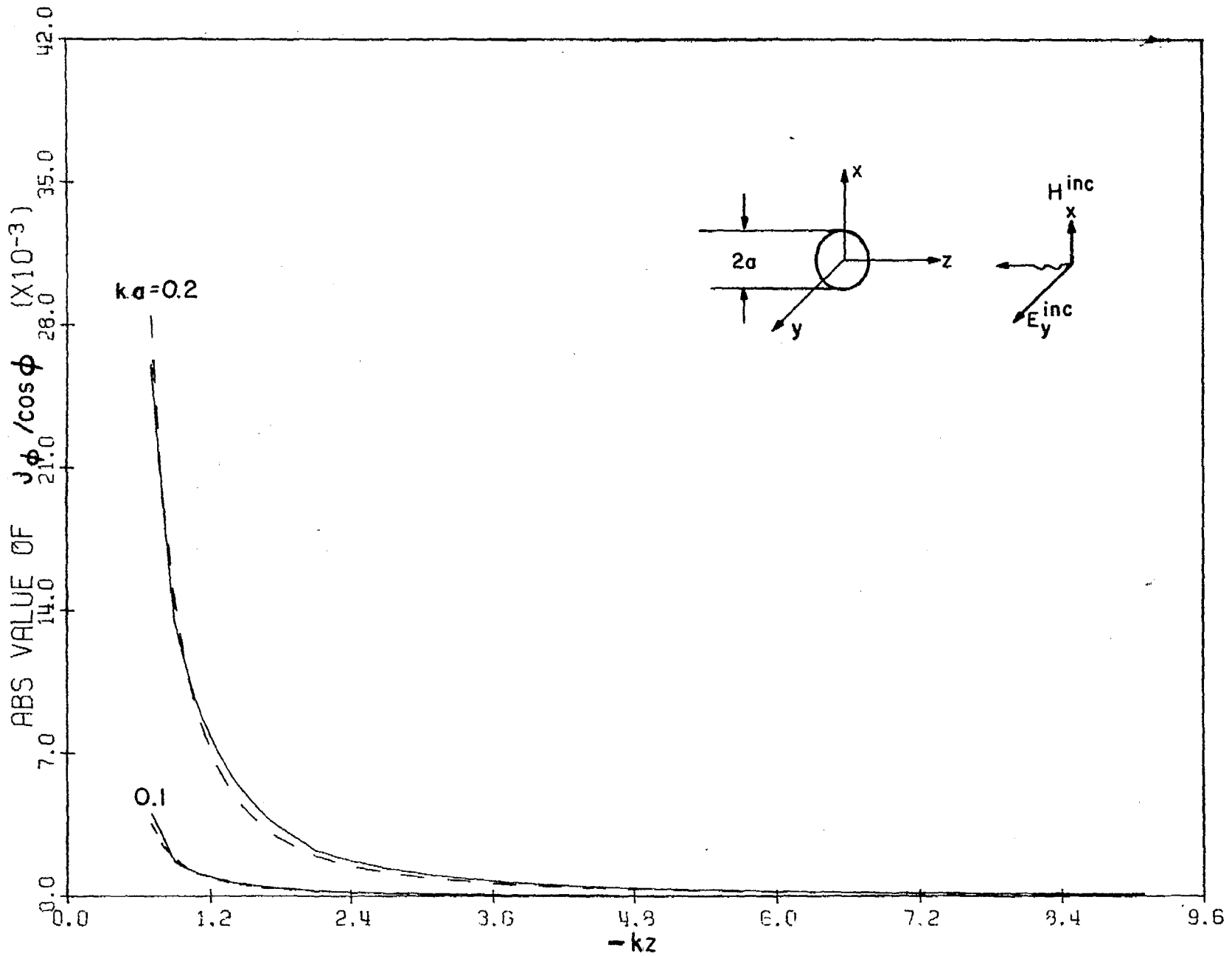


Figure 11a. Comparison of the absolute value of the circumferential current as computed from general formulas in Section 5 and from low-frequency approximations in Section 6

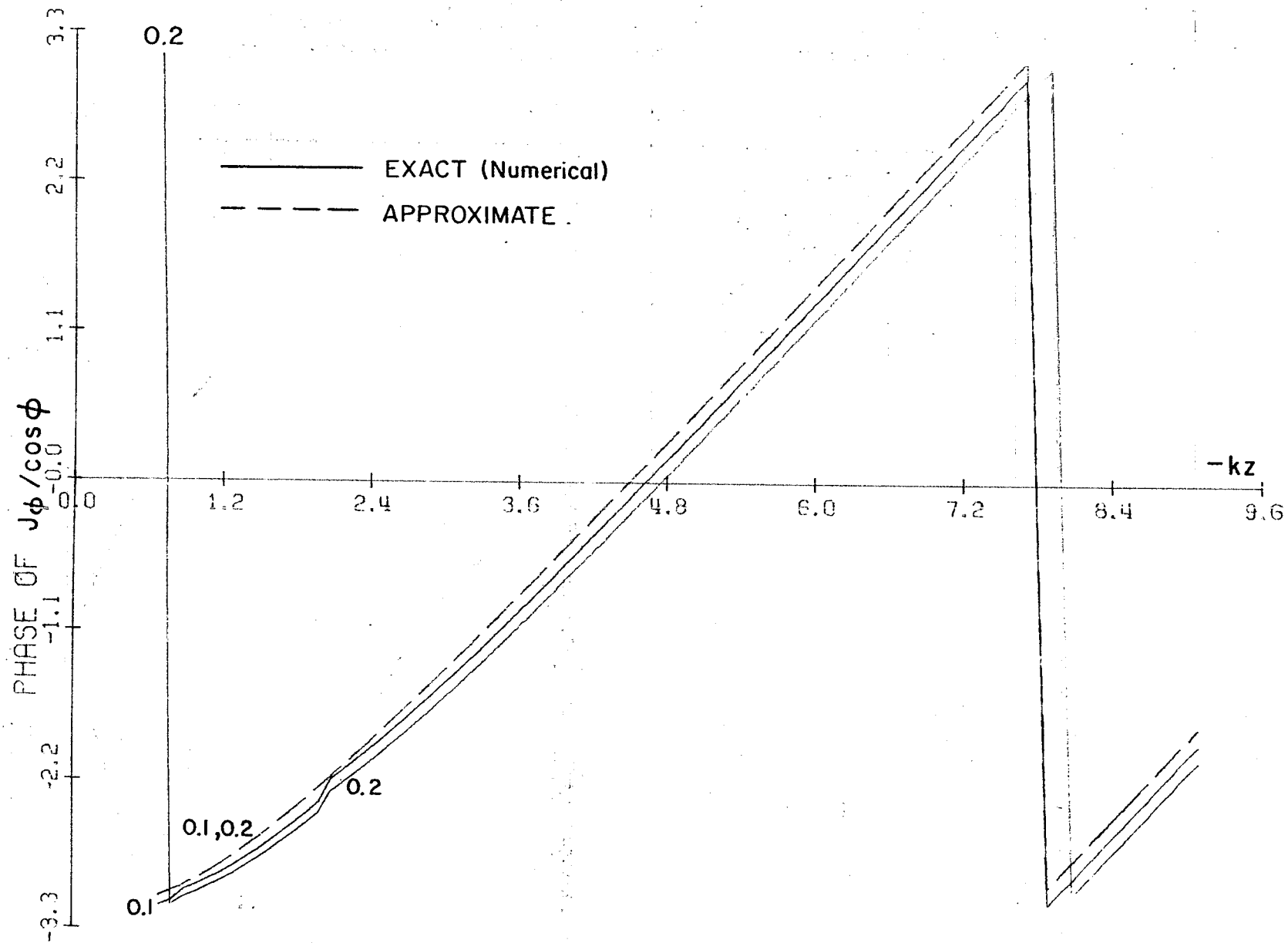


Figure 11b. Comparison of the phase of the circumferential current as computed from general formulas in Section 5 and from low-frequency approximations in Section 6

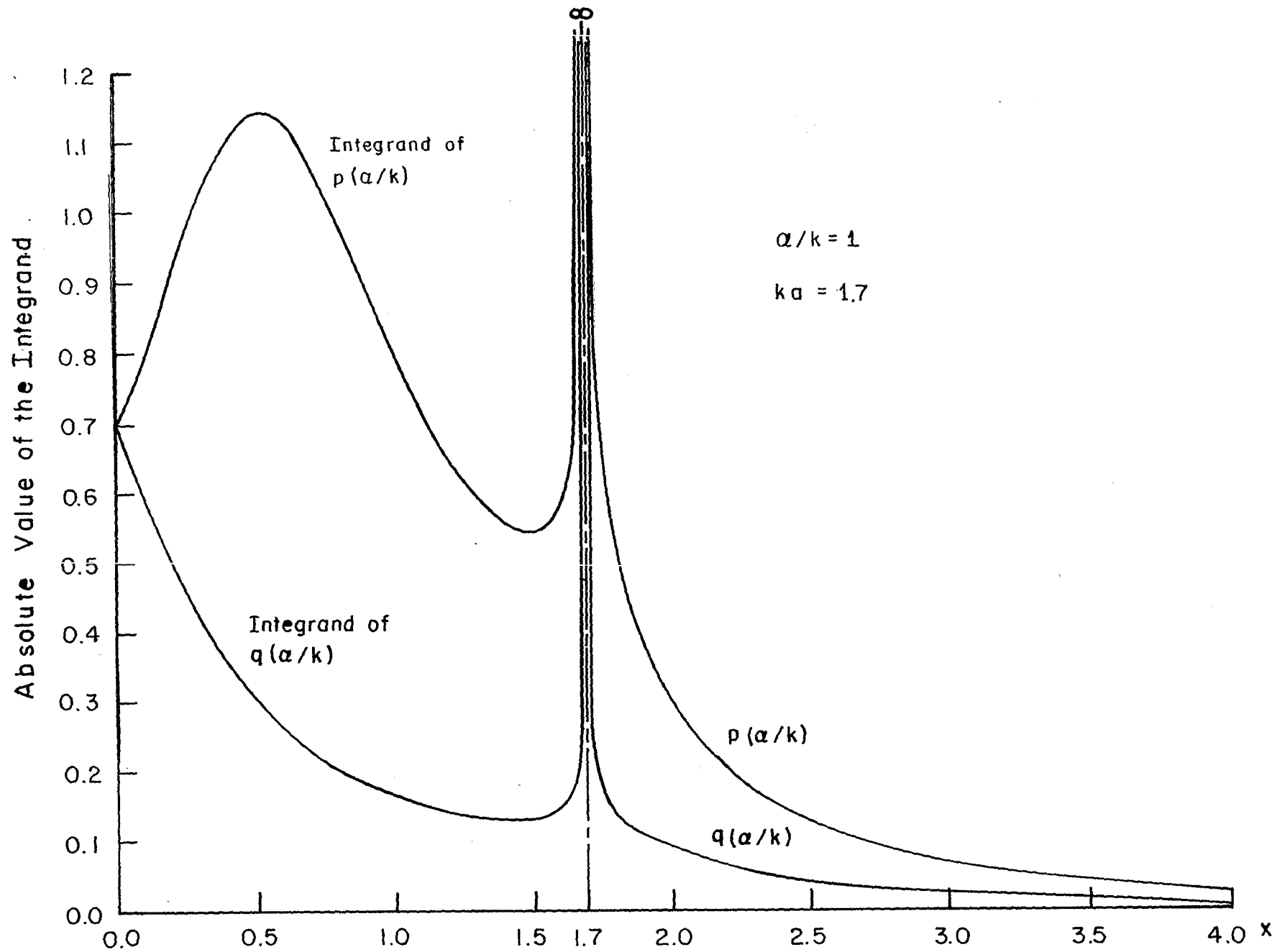


Figure 12. Variation of the absolute value of the integrand of $q(\alpha/k)$ in (A.7) and the integrand of $P(\alpha/k)$ in (A.22), versus x for typical values of (α/k) and (ka)

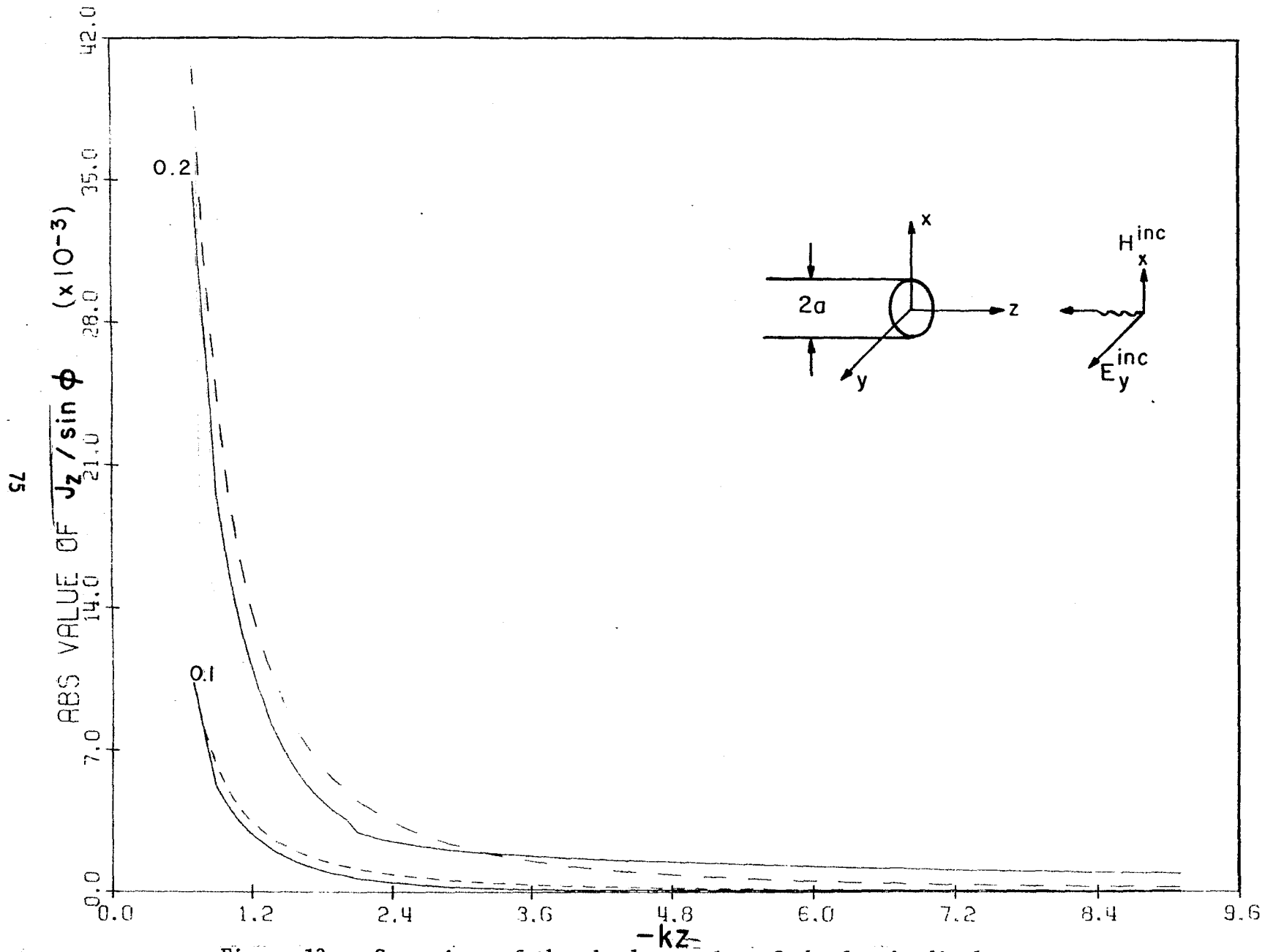


Figure 13a. Comparison of the absolute value of the longitudinal current as computed from general formula (A.39) and from low-frequency approximation formula (A.46)

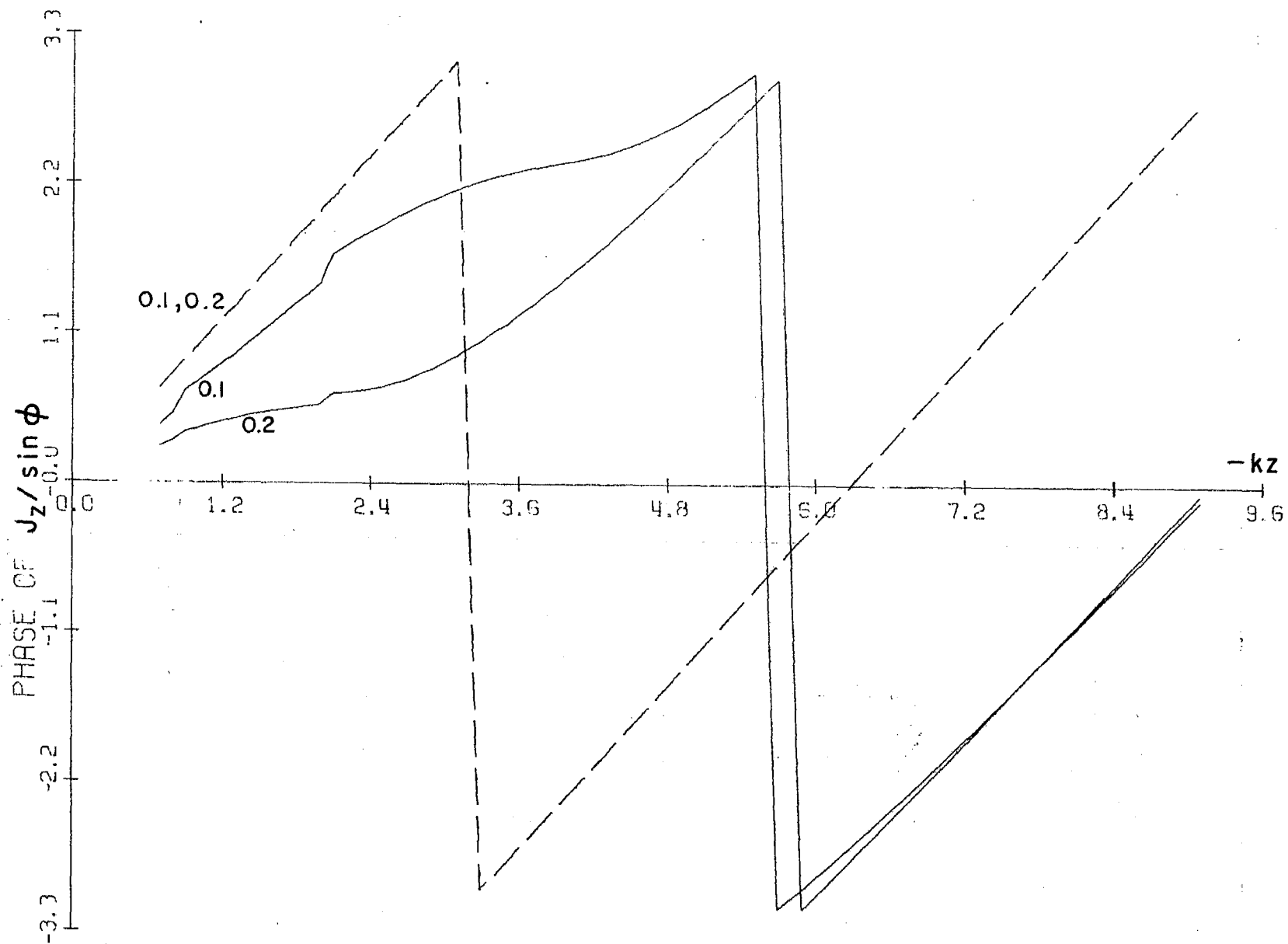


Figure 13b. Comparison of the phase of the longitudinal current as computed from general formula (A.39) and from low-frequency approximation formula (A.46)